Accepted version

Quantitative Studies of the Far-UV, UV and Optical Spectra of Late O and Early B-type Supergiants in the Magellanic Clouds[1]

C. J. Evans[2], P. A. Crowther[3], A. W. Fullerton[4,5], D. J. Hillier[6]

ABSTRACT

We present quantitative studies of 8 late O and early B-type supergiants in the Magellanic Clouds using far-ultraviolet *FUSE*, ultraviolet *IUE*/*HST* and optical VLT-UVES spectroscopy. Temperatures, mass-loss rates and CNO abundances are obtained using the non-LTE, spherical, line-blanketed model atmosphere code of Hillier & Miller (1998). We support recent results for lower temperatures of OB-type supergiants as a result of stellar winds and blanketing, which amounts to ∼2000 K at B0 Ia. In general, Hα derived mass-loss rates are consistent with UV and far-UV spectroscopy, although from consideration of the S IV $\lambda\lambda$1063-1073 doublet, clumped winds are preferred over homogenous models. AV 235 (B0 Iaw) is a notable exception, which has an unusually strong Hα profile that is inconsistent with the other Balmer lines and UV wind diagnostics. We also derive CNO abundances for our sample, revealing substantial nitrogen enrichment, with carbon and oxygen depletion. Our results are supported by comparison with the Galactic supergiant HD 2905 (BC0.7 Ia) for which near-solar CNO abundances are obtained. This bolsters previous suggestions that

[1]Based on observations made with the NASA-CNES-CSA Far Ultraviolet Spectroscopic Explorer. FUSE is operated by The Johns Hopkins University under NASA contract NAS5–32985. Also based in part on observations collected at the European Southern Observatory Very Large Telescope in program 67.D-0238, plus archival data obtained with the NASA-ESA Hubble Space Telescope and the NASA-ESA-PPARC International Ultraviolet Explorer.

[2]Isaac Newton Group of Telescopes, Apartado de Correos 321, 38700 Santa Cruz de la Palma, Canary Islands, Spain

[3]Dept. of Physics & Astronomy, Hounsfield Road, University of Sheffield, Sheffield S3 7RH, UK

[4]Dept. of Physics & Astronomy, University of Victoria, P.O. Box 3055, Victoria, BC, V8W 3P6, Canada

[5]Center for Astrophysical Sciences, Dept. of Physics & Astronomy, The Johns Hopkins University, 3400 N. Charles Street, Baltimore, MD 21286

[6]Department of Physics & Astronomy, University of Pittsburgh, 3941 O'Hara Street, PA 15260

"normal" OB-type supergiants exhibit atmospheric compositions indicative of partical CNO processing.

Subject headings: stars: early-type – stars: ultraviolet – stars: fundamental parameters – stars: mass-loss

1. Introduction

The *Far Ultraviolet Spectroscopic Explorer* (*FUSE*) satellite (Moos et al. 2000) has provided an opportunity to study populations of early-type stars in the Milky Way and Magellanic Clouds in the 900-1200Å region. Spectral atlases of *FUSE* observations of O and early B-type stars have recently been presented by Pellerin et al. (2002) and Walborn et al. (2002). The principal scientific motivation for such observations is the comparison of stellar winds from early-type stars in different metallicity (Z) environments. The predicted theoretical dependence of radiatively driven winds from massive stars is well documented, such that $\dot{M}(\mathrm{Z}) \propto Z^{0.5-0.7}$ (Kudritzki, Pauldrach & Puls, 1987; Vink, de Koter & Lamers, 2001); observationally this has yet to be firmly established. The precise sensitivity of mass-loss to metallicity for early-type stars is keenly sought as it is a necessary ingredient for stellar evolution models (and in turn evolutionary synthesis models).

Towards this goal, we initiated a program to obtain high-quality optical observations with the UV-Visual Echelle Spectograph (UVES) at the Very Large Telescope (VLT) for the Magellanic Cloud targets in our *FUSE* Principal Investigator programmes. We have focused particularly on the Clouds to avoid contamination associated with the high column densities of H_2 typical of sightlines to Galactic OB-type stars (e.g., Pellerin et al. 2002) and to minimize the effect of uncertainties in the distances to the targets on the atmospheric analysis. At the same time, so-called "unified" stellar atmosphere models are now available which allow for the spherical extension of supergiants and treat line blanketing by metal species in a reasonably thorough manner.

Crowther et al. (2002; hereafter Paper I) presented the first study of the present series for four Magellanic Cloud O-type supergiants, employing the model atmosphere code CMFGEN (Hillier & Miller, 1998). These extreme supergiants (all were of luminosity class Ia^+) were specifically chosen to test previously adopted stellar temperatures for O-type stars, for which Fullerton et al. (2000) had questioned the previous plane-parallel, unblanketed results (e.g., Vacca et al. 1996). Indeed, substantially lower temperatures were derived for these extreme supergiants. The combination of very strong stellar winds together with metal line blanketing led to temperatures 15–20% lower than those from plane-parallel models composed solely

of hydrogen and helium. Downward revisions were also found for Galactic O-type dwarfs (Martins et al. 2002) and supergiants in the Galactic cluster Cyg OB2 (Herrero et al. 2002). For our second paper we have therefore chosen to study O-type stars with luminosity classes in the range II to Ia^+, to better address the question of the stellar temperature scale. We have also extended our sample to include early B-type supergiants, thereby providing an overlap between Paper I and the recent results of Trundle et al. (2004).

In Paper I, CNO abundances of extreme O-type supergiants were found to differ greatly from those inferred from nebular and stellar studies in the Magellanic Clouds. Nitrogen was strongly enhanced, with carbon (and oxygen) moderately depleted, suggestive of mixing of unprocessed and CNO-processed material at their surfaces. These results were supported by a companion study by Hillier et al. (2003) which used identical techniques. They found unprocessed CNO abundances for AV 69 [OC7.5 III((f))] and partially CNO-processed material in AV 83 (O7 Iaf^+). Therefore, morphologically normal OB stars appear to show evidence for moderate levels of chemical processing. This new study allows us to examine CNO abundances in less extreme supergiants.

The issue of clumping in early-type stars was raised in Paper I and by Hillier et al. (2003). In order to reconcile the optical Hα and far-UV P V $\lambda\lambda$1118-28 wind diagnostics, either clumped winds or a reduced phosphorus abundance was required. Massa et al. (2003) arrived at similar conclusions from a study of *FUSE* observations of O-type stars in the LMC. The question of clumping, and hence reduced mass-loss rates for OB-type stars, is an important one, although the uncertain abundance of phosphorus in the interstellar medium (ISM) is a major limitation. In contrast, we shall suggest that S IV $\lambda\lambda$1062-73 is an analogue of P V $\lambda\lambda$1118-28 amongst late O and early B-type supergiants, for which the ISM elemental abundance is well known (e.g., Russell & Dopita 1992). This permits firmer conclusions regarding clumping in the winds of early-type stars.

As in Paper I, the *FUSE* data are complemented by UV spectra from the *International Ultraviolet Explorer* (*IUE*) telescope and the *Hubble Space Telescope* (*HST*) archives, together with optical data from UVES. The observational data are presented in §2, followed by a description of our methods in §3 and results for each of our targets stars in §4, except AV 235 which is discussed separately in §5. In §6 we discuss the CNO abundances derived for our targets and also present an analysis of the Galactic BC-type supergiant HD 2905 to provide a test of our methods. Finally, we discuss the implications of our results for published temperature calibrations and give a comparison of our observationally derived mass-loss rates with theoretical predictions.

2. Observations

2.1. Optical data

Basic observational parameters for the target stars are given in Table 1. High resolution optical spectra of HDE 269050, AV 235, 372 and 469 were obtained during 2001 September 27-29 with UVES (using the #2 dichroic) at the VLT. The standard blue-arm setting (λ_c = 4370 Å) with a single 2×4k EEV CCD (15×15μm pixels), gave a spectral coverage of λ3770–4950 Å. A non-standard setting (λ_c = 8300 Å) was used for the red-arm, with an identical EEV CCD giving wavelength coverage of λ6400–8200 Å. The 2-pixel resolution in the Hα region was 0.09 Å. Further echelle orders into the far-red (to ∼10000 Å) were also observed simultaneously with an MIT CCD, though due to poor signal-to-noise these data are not used here. In addition, UVES spectra of HDE 269896, AV 70, 456 and 488 were kindly provided by Dr. Lex Kaper from observations on 2001 September 24, obtained for a study of Diffuse Interstellar Bands (Ehrenfreund et al., 2002). The settings for these observations were slightly different but the overall spectral coverage is comparable (see Table 2), except for AV 456 for which the λ4520–4660 Å region was not available.

The data were cleaned of cosmic rays, bias corrected, flat fielded and optimally extracted in IRAF[1] (v2.11). The echelle blaze profile was removed by fitting a two-dimensional surface to the orders and then dividing it into the data using a routine developed by Prof. Ian Howarth (private communication) for the Starlink program DIPSO.

With the exception of AV 456, spectral classifications for our targets are given by Walborn, et al. (1995, 2002). Previous classifications for AV 456 include O9.5 I (Fitzpatrick 1985), B0 (Nandy, Morgan & Houziaux 1990), O9.5 V (Massey et al. 1995) and O9.5 Ib (Evans et al. 2004). New digital data for AV 456 are presented in Figure 1. Unfortunately the wavelength coverage in the UVES data is somewhat limited so the spectrum is accompanied by an intermediate-resolution spectrum obtained using the two-degree field facility (2dF) at the Anglo-Australian telescope (AAT) from Evans et al. (2004). To assist classification the UVES data were Gaussian-smoothed and rebinned to an effective resolution of 1 Å FWHM. For comparison, the UVES spectrum of AV 70 is also shown (classified as O9.5 Ibw by Walborn et al. 2002). Note the strong similarity between the two UVES spectra, particularly the ratio of He II λ4200 to He I λ4144 and the intensity of the He II λ4686 absorption; for these reasons we classify AV 456 as O9.5 Ibw.

[1]IRAF is distributed by the National Optical Astronomy Observatories, which are operated by the Association of Universities for Research in Astronomy, Inc., under cooperative agreement with the National Science Foundation.

Morphologically, the ON-type star in our sample, HDE 269896 (ON9.7 Ia$^+$) is very similar to Sk−66°169 (O9.7Ia$^+$) from Paper I. Digital data for HDE 269896 were published by Walborn & Fitzpatrick (1990) and for Sk−66°169 by Fitzpatrick (1991). A useful illustration of the ON/OC phenomenon in high-quality digital data is given by Walborn & Howarth (2000). The ON classification for HDE 269896 arises because of the approximately equal N III λ4640 and C III λ4650 intensities, compared to the "normal" case in Sk−66°169, where the C III absorption is much stronger; the N III λ4097 line is also stronger with respect to Hδ in HDE 269896. We note that the peak intensity of the Hα emission for HDE 269896 is larger than that for Sk−66°169, suggesting a greater mass-loss rate.

2.2. Far-UV and UV spectroscopy

Far-UV spectra for the majority of our targets were obtained from *FUSE* Principal Investigator Team programs P117 (P.I.: J. B. Hutchings) and P103 (P.I.: K. R. Sembach); total exposure times are given in Table 2. Additionally, AV 70 was observed as part of program B090 (P.I.: J. M. Shull) and AV 456 for program Q107 (P.I.: R. Ferlet). As in Paper I, data from each *FUSE* detector were processed using the CALFUSE 2.0.5 pipeline and then subsequently aligned, merged and resampled to a constant wavelength step of 0.13 Å as described by Walborn et al. (2002).

To augment the *FUSE* spectra we relied on UV spectroscopy of our targets from the *IUE* and *HST* archives (as shown in Table 2). The majority of our targets were observed with the *IUE* satellite using the large aperture in the short-wavelength (SWP) channel at high dispersion (HIRES). For AV 469 and 372 we have used *HST* Faint Object Spectrograph (FOS) spectra from *HST* programme 5444 (P.I.: C. Robert), details of which can be found in Leitherer et al. (2001).

The reddening in the direction of AV 456 is much larger than that for the other SMC targets (see Table 1). Indeed, the *FUSE* spectrum of AV 456 contains such significant molecular hydrogen absorption that it is essentially devoid of useful stellar features apart from the C III λ1176 multiplet. AV 456 was observed with *IUE*, however this was at low dispersion (LORES) meaning that our far-UV and UV coverage for this star is relatively limited in comparison to the rest of the sample.

3. Analysis method

A comparison between unblanketed, plane-parallel results and line-blanketed, spherical results for four O-type supergiants was presented in Paper I; further comparisons are not undertaken here. In contrast, Bouret et al. (2003) demonstrated good agreement between *fully* line-blanketed, plane-parallel models computed with TLUSTY and CMFGEN models for O-type dwarfs in the SMC, for which the effects of the stellar wind on the emergent spectrum are substantially smaller.

Our methods for the determination of intrinsic parameters were largely identical to the approach taken in Paper I and by Hillier et al. (2003). We varied the mass-loss rate and the velocity law (as characterized by the exponent β) until the Hα profile was best reproduced in terms of intensity and morphology, subsequently adjusting the stellar temperature to match the intensities of the He II λ4200/4542 and He I lines. However, He II becomes exceptionally weak for the B-type supergiants in our sample so the relative intensities of Si IV λ4089 and Si III λ4553-68-75 lines were used instead as primary temperature indicators for these stars. The alternative temperature diagnostics were generally in excellent agreement.

Terminal velocities, v_∞, were primarily determined from $v_{\rm black}$ (e.g., Prinja, Barlow, & Howarth, 1990) of the N III λ990 doublet (largely uncontaminated from molecular hydrogen), with consideration to other saturated lines in the far-UV. Terminal velocities for each of our targets are listed in Table 3.

A firm determination of the helium content of extreme supergiants is extremely difficult (e.g., Hillier et al. 2003) so, following the arguments from Paper I, the He abundance (by number) was fixed for our most luminous targets at He/H = 0.2. For the less luminous supergiants, we initially assume He/H = 0.2, though we have explored alternative abundances. As mentioned in Paper I, helium abundance differences of $\sim$0.1 are not found to affect the derived temperatures significantly, although an additional uncertainty is introduced into the derived mass-loss rate.

CNO abundances were varied to fit the relevant optical lines, with a typical accuracy of $\sim$0.3 dex. Solar CNO abundances were taken from Grevesse & Sauval (1998) except oxygen, which was set at log(O/H)+12 = 8.66 (Asplund, 2003). Abundances of other metallic elements were fixed at $0.4Z_\odot$ (LMC) and $0.2Z_\odot$ (SMC), e.g., Russell & Dopita (1992). The primary diagnostic line used for determination of the nitrogen abundance was N III λ4097, with consideration of N II λ3995 and the N III λ4640 blend which are less sensitive to abundance changes. Oxygen and carbon abundances were also determined from consideration of the optical lines; O II λ4415–17 and λ4069–4092 provided useful constraints on the oxygen abundance, whilst C II λ4267 together with C III λ4647–51 (blended with O II) were used

for carbon.

Another physical parameter that affects the analysis is the rotational velocity of the star. This redistributes the flux in a given line, with the net result that peak absorption and emission intensities are reduced. Work is underway by Hillier and co-workers to include the effects of rotation on stellar wind lines (see discussion in Hillier et al. 2003; also Busche 2001, Busche & Hillier 2004). Here we limited ourselves to the standard procedure of convolving the synthetic spectrum with a rotational broadening profile. Following the method of Herrero et al. (1992), we estimate $v\sin i$ values using weak metal lines (e.g., those of Si III) and the weaker He I lines (e.g., λ4009). The model spectra were convolved initially by $v\sin i = 80$ kms^{-1} (rotational velocities in early-type supergiants are generally low, e.g., Howarth et al. 1997) and, if necessary, then changed to match the breadth of the metal/He I lines. Adopted $v\sin i$ values are given in Table 3.

The model atoms used for our CMFGEN calculations were similar to those used for the Sk−66°169 in Paper I (see Table 4 therein). Our flux calculations allow for a radially dependent microturbulence[2] (ξ) as described by Hillier et al. (2003). In Paper I the most consistent fit for Sk-66°169 (O9.7 Ia$^+$) was achieved with $\xi = 20$ kms^{-1}; the same value was found by Villamariz et al. (2002) in their analysis of the Galactic O9.5 Ib supergiant HD 209975. For the present sample we initally assume $\xi = 20$ kms^{-1}, with other values considered if consistent fits are not found for the helium and silicon lines.

4. Analyses of Magellanic Cloud OB-type supergiants

Stellar parameters derived from comparisons of the observed spectra with CMFGEN models are summarized in Table 3. Three stars (AV 235, HDE 269050 and HDE 269896) have strong stellar winds for which unique values of $\dot{M}$ and β are determined. In contrast, the winds of our remaining targets are much weaker and, as in the case of AV 69 (Hillier et al. 2003), there can be some degeneracy between β and $\dot{M}$ (as noted by e.g., Puls et al. 1996) leading to a range of derived parameters for AV 456 and 469. The determination of the best fitting model for each star is subjective, primarily driven by matching the observed Hα profile for each star.

In most cases, agreement between the Hα derived mass-loss rate and blue visual region is excellent, with the exception of He II λ4686 (formed both in the photosphere and in

[2]In CMFGEN this adopted value is technically $\xi_{\rm min}$, the microturbulence at the base of the wind, which increases with radius to $\xi_{\rm max} = 100$ kms^{-1} at v_∞.

the transition zone at the base of the wind). At the temperatures and luminosities of the current sample λ4686 demonstrates a wide range of behaviour, i.e., from strong absorption (e.g., AV 70, see Figure 3) to strong emission (HDE 269896). This line is strongly sensitive to both the atmospheric extension and the photospheric microturbulence; larger turbulent velocities drive the line more strongly into emission. In comparison with other diagnostic lines, the behaviour of the model λ4686 profiles suggests that, for this line, we are perhaps limited by the adoption of a depth independent photospheric turbulence.

UV and far-UV comparisons are generally successful, as we shall discuss later. However, for AV 235 the agreement between Hα and the other Balmer lines is extremely poor; it is discussed separately in §5. The remaining stars are now discussed in turn, with synthetic spectra compared to optical observations in Figures 2–4. One further unresolved problem is common to most stars. As revealed in Figure 4, there is often a substantial $\sim$50–100 kms^{-1} offset between the apparent radial velocity shift of the observed Hα profile compared to that of the He I λ6678 line. The radial velocity of the He I line is more in keeping with the blue data (see Table 1), i.e., the peak of the Hα emission is significantly discrepant from its expected wavelength in the *observed* spectrum. Checks of the UVES observations with conventional long-slit spectra taken with the 2.3m Australian National University (ANU) telescope, confirm the wavelength of the observed Hα feature in all cases, and measurements of the He I λ7065 line are consistent with those at λ6678. Although the effect was less significant ($\sim$40 kms), a similar offset was also present in the spectrum of AV 83 (Hillier et al. 2003).

4.1. AV 469 [Sk 148, O8.5 II((f))]

We derive $T_{\rm eff} = 33$ kK, $\log(L/L_{\odot}) = 5.50$ and $v_{\infty} = 1550$ kms^{-1} for AV 469, very similar parameters to those found for AV 69 [OC7.5 III((f))] by Hillier et al. (2003). The Hα profile of AV 469 (see Figure 4) is strongly in absorption and there is some degeneracy between $\dot{M}$ and β. Models were calculated for β exponents in the range 0.85–1.75, varying the mass-loss rate to optimally match the Hα profile. The best fitting model has $\dot{M}$ =1.3$\times10^{-6}$ $M_{\odot}$ yr^{-1} with $\beta = 1.0$, although reasonable fits can also be obtained adopting $\beta = 0.85$ and 1.25, resulting in $\dot{M}$ values of order 20% higher and lower respectively. The other derived parameters remain invariant to such changes in β.

As with our other targets these models assume He/H = 0.2; lower He abundance models were generated but provided less consistent fits to the helium lines. The nitrogen abundance is fixed using N III λ4097, revealing a mass fraction (relative to solar) of ϵ(N/N$_{\odot}$)$\sim$1.5, indicating a large enhancement when compared to the SMC interstellar medium. We are

unable to match the observed 4634–41 N III emission lines, although in our models they are somewhat "filled-in" (cf. the absorption in our models for other stars, see Figure 3). The carbon abundance derived using C III λ4650 for AV 469 is $\epsilon(\mathrm{C/C_\odot}) = 0.03$, providing strong evidence of depletion compared to the nebular abundances. As one might expect given the relatively high stellar temperature, the O II λ4415-17 doublet is not detected in AV 469, so no firm abundance determination was possible.

4.2. AV 372 (Sk 116, O9 Iabw)

From inspection of the Hα profile (see Figure 4) AV 372 clearly has a very weak wind. The final model has $T_{\rm eff}$= 28 kK, $\log(L/L_\odot) = 5.62$ and $\dot{M}$= 1.0×10^{-6} $M_\odot$ yr^{-1} with β = 2.25 and a helium number abundance of He/H = 0.15. The terminal velocity from the *FUSE* spectrum is v_∞ = 1550 kms^{-1}, identical to that found from *HST* UV spectra by Prinja & Crowther (1998). We are unable to simultaneously match the observed absorption and weak emission; lower values of β with a higher mass-loss rate (and vice versa) do not successfully improve agreement with the observed profile. As mentioned earlier, there is a velocity offset between Hα and the He I lines in the red UVES data, in this case ∼100 kms^{-1}.

Again, nitrogen is strongly enhanced relative to the ISM of the SMC, with $\epsilon(\mathrm{N/N_\odot})$ = 0.6. The O II λ4415-17 doublet is not visible in the AV 372 UVES spectrum, thus the λ4650 feature is expected to originate largely from C III, leading to the carbon abundance of $\epsilon(\mathrm{C/C_\odot}) = 0.05$.

4.3. AV 70 (Sk 35, O9.5 Ibw)

The Hα profile in AV 70 (see Figure 4) has a double emission peak with significant central absorption, a feature commonly seen in Be-type stars (e.g., Slettebak, 1988). We are unable to reproduce this feature using our current 1D method and limit ourselves here to simultaneously matching the redward emission and the blue-region optical lines. The parameters found for AV 70 are $T_{\rm eff}$= 28.5 kK, $\log(L/L_\odot) = 5.68$, $\dot{M}$= 1.5×10^{-6} $M_\odot$ yr^{-1} with β = 1.75. Again note the observed velocity offset in Figure 4 between Hα and He I λ6678 of ∼100kms^{-1}.

As with AV 469 and AV 372, nitrogen is over-abundant in AV 70, with $\epsilon(\mathrm{N/N_\odot}) \sim 0.9$, whilst carbon is deficient, $\epsilon(\mathrm{C/C_\odot}) = 0.03$. Given the relatively high stellar temperature for the preferred AV 70 model, the O II λ4415-17 is very weak (if present at all) and the derived oxygen abundance is given as an upper limit.

We are unable to match all of the observed helium and silicon features simultaneously for AV 70; the Si IV absorption lines in the final model are too strong (see Figure 2). The adopted microturbulence (i.e., $\xi = 20$ kms^{-1}) was that found from consideration of the helium lines by, e.g., Villamariz et al. (2002). In early B-type stars the microturblent velocity is generally determined from silicon (and oxygen) lines and the result values are typically lower ($\sim$10 kms^{-1}, e.g., McErlean et al. 1999). Calculation of the formal solution for AV 70 with $\xi = 10$ kms^{-1} gives good agreement for the Si III/IV and He II lines, with the consequence that the predicted intensity of the He I lines is generally too small. This highlights the potentially different values of ξ obtained from separate elements, as noted by McErlean et al. and Vrancken et al. (2000) in reference to results from silicon and oxygen.

4.4. AV 456 (Sk 143, O9.5 Ibw)

As discussed in §2.1, the blue optical spectrum of AV 456 is strikingly similar to that of AV 70 and one might therefore anticipate comparable stellar parameters. However, the Hα profiles of the two stars differ substantially (see Figure 4). Due to the high interstellar extinction, we were unable to determine v_∞ for AV 456 using the N III and other far-UV lines, so we adopt the same terminal velocity as for AV 70 (recall only LORES *IUE* datasets are available for this star).

An optimal fit was obtained for $T_{\rm eff}$= 29.5 kK and $\dot{M} = 0.7{\times}10^{-6}$ $M_\odot$ yr^{-1} with $\beta = 1.75$. The blue visual data for AV 456 are omitted from Figures 2 and 3 as they are much noisier than those for the other targets.

A helium number abundance of He/H = 0.1 is preferred for AV 456, although in this instance such differences in helium abundance (cf. AV 70) should not be considered significant. Recall that the Hα profile for AV 70 is poorly reproduced in our spherical 1D model – it is possible that a circumstellar disk or shell leads to the observed emission superimposed on the stellar absorption profile. This would lead to an artificially high mass-loss rate and therefore the higher helium abundance. From inspection of the raw data the He I lines in AV 70 are slightly broader and shallower than in AV 456, accounting for the slight difference in the adopted $v\sin i$ values.

Due to the lack of optical data in the λ4500-4700 Å region, a thorough abundance analysis is not possible for AV 456, although $\epsilon({\rm N/N_\odot}) = 0.6$ is derived for nitrogen from N III λ4097. The O II λ4415-17 doublet (if present) is indistinguishable from the noise and so the upper limit to the oxygen abundance is again $\epsilon({\rm O/O_\odot}) \leq 0.2$.

4.5. HDE 269896 (Sk–68°135, ON9.7 Ia$^+$)

The terminal velocity found from fits to the *FUSE* lines (v_∞ = 1350 kms^{-1}) for HDE 269896 is somewhat larger than that found by Massa et al. (2003) from analysis of *IUE* spectra (v_∞ = 1050 kms^{-1}). For consistency with the methods employed for the rest of the current sample (and those in Paper I) we adopt the value found from the *FUSE* data.

HDE 269896 is significantly more luminous than its spectroscopic twin (Sk−66°169) with $\log(L/L_\odot) = 5.97$. We derive a temperature of $T_{\rm eff}$ = 27.5 kK, with a mass-loss rate of $\dot{M}$= 7.5×10^{-6} $M_\odot$/yr^{-1} and a relatively large wind exponent of β = 3.5 (i.e., a comparatively slow radial acceleration). We find evidence of nitrogen enhancement with ϵ(N/N$_\odot$) ∼ 2, whilst both carbon and oxygen are metal poor with ϵ(C/C$_\odot$) ∼ 0.06 and ϵ(O/O$_\odot$) ∼ 0.17. A comparison between HDE 269896 and Sk−66°169 is made in Sect. 6.

4.6. HDE 269050 (Sk–68°52, B0 Ia)

The derived parameters for HDE 269050 are $T_{\rm eff}$= 24.5 kK, $\log(L/L_\odot)$ = 5.76, $\dot{M}$= 3.2×10^{-6} $M_\odot$ yr^{-1}with β = 2.75. The discrepancy between the radial velocities in the observed Hα profile and He I λ6678 is also present in HDE 269050, though its magnitude is lower (∼60 kms^{-1}, see Figure 4). Again there is evidence of significant CNO-processing with ϵ(C/C$_\odot$) = 0.15 ϵ(N/N$_\odot$) = 3.7 and ϵ(O/O$_\odot$) = 0.5, the latter based on optical O II diagnostics.

4.7. AV 488 (Sk 159, B0.5 Iaw)

The redward emission in the Hα profile of AV 488 permits a unique determination of $\dot{M}$ and β. The final derived parameters for AV 488 are $T_{\rm eff}$= 27 kK, $\log(L/L_\odot)$ = 5.74, $\dot{M}$ = 1.2×10^{-6} $M_\odot$ yr^{-1} with β = 1.75, and He/H = 0.20. The terminal velocity from the *FUSE* data is v_∞ = 1250 kms^{-1}, compared to previous determinations of 1300 kms^{-1} (Haser 1995) and 1040 kms^{-1} (Prinja & Crowther 1998). There is also a velocity shift between He I λ6678 and Hα of ∼60 kms^{-1}(see Figure 4), though in the opposite sense to that seen in our other targets, i.e., the observed Hα profile is apparently consistent with a lower radial velocity than that from He I. Models were also calculated with He/H = 0.1 by number; the derived parameters of the best fitting model were identical, with the exception that $\dot{M}$ = 1.0×10^{-6} $M_\odot$ yr^{-1} and the quality of the fits to the He I lines was slightly diminished. Once again, based on several N II, C II and O II lines, AV 488 shows evidence of partial CNO-processing, with ϵ(C/C$_\odot$) = 0.04, ϵ(N/N$_\odot$) = 1.2 and ϵ(O/O$_\odot$) = 0.17.

4.8. UV and far-UV comparisons: Further evidence for clumping in OB-type stars?

Thus far, we have carried out a comparison between synthetic *optical* spectra and observations. As in Paper I, we now consider how well these optically derived parameters reproduce the UV and far-UV spectral features. Successes and failures of the present models are generally common to stars of each spectral type (recall that AV 235 is discussed separately). The N V $\lambda\lambda$1238–42 and O VI $\lambda\lambda$1032–1038 doublets are purposefully omitted from these comparisons since these are super-ions produced by X-rays in late O and early B-type stars (see Paper I). Furthermore, HDE 269896 is closely reminiscent of Sk−66°169 from Paper I and is not discussed here.

In Figure 5 we compare model spectra of four representative targets with *IUE* observations, covering $\lambda\lambda$1250–1800. In general, the UV comparison supports the stellar parameters derived from our optical analysis, although recall from Paper I that UV wind diagnostics provide relatively poor discriminants between different models for O-type spectra (although the photospheric lines are more useful, e.g., the Fe IV/Fe V ratio). The principal spectral features in the *IUE* range are Si IV $\lambda\lambda$1393–1402 and C IV $\lambda\lambda$1548–51, together with the iron "forest" redward of λ1500. The optically derived models match the observations reasonably well, with the exception of the Si IV P-Cygni emission, over-predicted in many of our targets. The UV plays a greater diagnostic role for early B supergiants, in which Massa (1989) found that some of the UV silicon lines are sensitive to temperature and luminosity. For the later subtypes in our sample (i.e., HDE 269050 and AV 488) there is good agreement in the Si III lines discussed by Massa (namely λ1294, 1299 and 1417), which offers further confidence in our derived temperatures.

Now we turn to the far-UV *FUSE* region, which proved much more useful for the O-type stars in Paper I. Unfortunately, interstellar molecular H_2 is rather more problematic for AV 488 and HDE 269050 with column densities of $10^{19-19.5}$ cm^{-2} (Tumlinson et al. 2002) but the principal spectral features remain relatively clear (see Figure 6). Many of the far-UV features (e.g., C III λ1176 and the O III λ1139-50-51-54 lines) are well reproduced by our (unclumped) models, however the P-Cygni emission is again over-predicted in some lines, e.g., C III λ977, N III λ991 and the S IV λ1062–1072 doublet.

Using the filling factor approach described in Hillier et al. (2003) we calculated clumped models to investigate the effects on our diagnostic lines. The volume filling factor was reduced from 100% to 10% (i.e., $f_\infty = 0.1$) with the velocity at which the clumping is initiated (v_{cl}) set to 30 kms^{-1} (taken from the analysis of AV 83 by Hillier et al.). Matching the Hα profiles of our targets with clumped models typically necessitated mass-loss rates a factor of 3 lower, with all other input parameters largely unchanged.

Clumped models are also shown in Figure 6. Recall from Paper I that P V λ1118–28 was identified as a potential indicator of clumping in early-mid O-type stars, both AV 469 and 372 appear to again demonstrate this. We suggest here that for late O and early B-type stars S IV $\lambda\lambda$1062–1072 may offer a similar diagnostic; these lines will be sensitive to clumping as they are unsaturated and arise from the dominant ion of the species. In Figure 7 we show the S IV and P V region for AV 372 in more detail. In contrast to phosphorus, the present day ISM abundance of sulphur in the Magellanic Clouds is well known from both H II regions (e.g., Russell & Dopita 1992) and stars (e.g., Rolleston et al. 2003). With the sulphur abundance fixed, a moderately clumped wind leads to less discrepant emission P-Cygni emission and the morphology of the absorption components are better matched.

The role of clumping in the winds of Wolf-Rayet stars is well documented (e.g., Moffat et al. 1988; Hillier 1991); only more recently have such effects been considered in O and B-type stars. We conclude that it is likely that the winds of O and early B-type supergiants are clumped, with the best spectroscopic evidence revealed by unsaturated lines of dominant ions in the far-UV *FUSE* region. Massa et al. (2003) arrived at a similar conclusion based on their line profile analyses of *FUSE* observations of O-type stars in the LMC. Additional supporting evidence was offered by Hillier et al. (2003) who noted that unclumped models predict asymmetries in some UV photospheric lines that are not seen in the observations; these discrepancies are reduced by the inclusion of clumping. Intensive spectroscopic monitoring of both optical emission features (Eversberg et al. 1998) and UV lines (Prinja, Massa, & Fullerton, 2002) have already indicated that winds in early type stars are highly structured; hydrodynamic models (Owocki et al. 1988) and X-ray spectroscopy (Miller et al. 2002) also suggest wind clumping.

5. The peculiar case of AV 235 (Sk 82, B0 Iaw)

For seven of the eight program stars, we obtain reasonably good agreement between the synthetic far-UV, UV and optical spectra and observations; for AV 235 this is not the case. Following our usual method, i.e., selecting a mass-loss rate from Hα and temperature from photospheric helium or silicon diagnostics we derive the following parameters: $T_{\rm eff} = 24.5$kK, $\log(L/L_\odot) = 5.63$, $\dot{M} = 5.8 \times 10^{-6} M_\odot {\rm yr}^{-1}$ with a $\beta = 2.5$ velocity exponent. The synthetic spectrum from this model is compared to observations in Figure 8 (to permit a clearer comparison of the predicted profiles the 100 kms^{-1} offset between He I λ6678 and Hα has been removed). For this set of parameters, we obtained CNO abundances of $\epsilon({\rm N/N}_\odot) = 2.3$, $\epsilon({\rm O/O}_\odot) = 0.2$ and $\epsilon({\rm C/C}_\odot) = 0.02$. The helium lines are well fit by this model, as are the Si III and IV lines. However, it is clear that the predicted P Cygni emission profiles for

Hβ, Hγ are far too strong in emission, in spite of Hα matching well; clumping is not able to resolve these differences.

Turning to the UV, many of the wind features are again over-estimated (see Figure 9); they too suggest a much lower mass-loss rate and/or higher ionization than that obtained from fits to Hα. For example, N II and Al III are predicted strongly in emission (yet such features are not observed in B supergiants earlier than B0.7, e.g., Walborn, Parker, & Nichols, 1995) whilst the predicted C IV is too weak.

We therefore calculated models which reproduced the usual optical diagnostics, except that Hγ was now selected as the mass-loss diagnostic. In this case (shown in Figure 10) a significantly higher stellar temperature was required to reproduce the photospheric He and Si lines, i.e., $T_{\rm eff}$ = 27.5kK, $\log(L/L_{\odot})$ = 5.72, $\dot{M} = 4.0 \times 10^{-6} M_{\odot}{\rm yr}^{-1}$ with an adopted $\beta = 1.5$ ("AV 235 Hγ" in Table 3). The line wings of Hγ are now well matched (though the predicted core absorption is too large) and the overall optical agreement is equal to the Hα model with the exception that this line and Hβ are now severely underestimated.

A consequence of the hotter model is that many of the UV features are in better agreement with the observations, namely P IV, N II, Si III, C IV and Al III as shown in Figure 11. This solution appears to be more representative for the true metal ionization balance, although the theoretical S IV and Si IV profiles are still strongly overpredicted; clumped models help slightly but do not resolve the problems.

Both the intensity and morphology of the Hα emission agree in our VLT-UVES and ANU spectra. Additionally, the feature is identical in a CASPEC echelle spectrum taken using the ESO 3.6-m telescope in Oct. 1991 (Dr. Daniel Lennon, private communication), i.e., there is no obvious evidence for significant Hα variability. Thus, clumping aside, the Hγ/far-UV and Hα wind diagnostics indicate a discrepancy in mass-loss of at least a factor of two. Ultimately, all optical diagnostics for AV 235 can be reproduced in the case of a clumped, weak wind at $T_{\rm eff}$ =27.5kK, with the exception of Hα. It would seem that in this case at least our assumption of spherical symmetry is not valid.

6. CNO abundances

Derived CNO abundances (by number) for our present sample are given in Table 4, together with those from Paper I and Hillier et al. (2003). We also include H II region abundances from Russell & Dopita (1992), plus more recent stellar abundances in the SMC from Venn (1999).

AV 488 is in common with the quantitative analysis of Lennon et al. (1991), for which a lower temperature of 25 kK was obtained. Their photospheric analysis yielded CNO abundances of log(C/H)+12 = 7.3, log(N/H)+12 = 7.7 and log(O/H) = 7.7, within a factor of three of the present values.

In Table 4 we also present new results for Sk−66°169. In the course of this work it became apparent that the source of the He II λ4686 discrepancy for this target in Paper 1 was due mainly to the large adopted turbulent velocity in the model atmosphere calculation, to which λ4686 is very sensitive. This discovery led to revisions in the adopted parameters of Sk−66°169 (a hotter model of 27.5 kK is now preferred), which in turn affects the derived abundances. This now enables us to make a fully consistent comparison between the two O9.7-type stars.

Walborn (1976) suggested that it is the OBC-type stars that are least evolved, rather than the morphologically normal and OBN-types. We would therefore expect normal supergiants to show evidence for partial CNO processing. In general (e.g., Paper I) "normal" O and B-type supergiants exhibit evidence of nitrogen enrichment, together with carbon and oxygen depletion. In the current sample, this is especially evident for HDE 269896 in which C/N=0.008, versus C/N=0.075 in Sk−66°169 (and C/N=8 for the ISM), i.e., HDE 269698 appears to be more fully processed. In contrast, the only OBC-type star from the combined sample, AV 69 (Hillier et al. 2003) reveals normal SMC C/N abundances. Given that AV 69 is an O7.5 giant, we now discuss an OBC supergiant that has stellar parameters much closer to the present sample to verify our claims, with a particular emphasis on the nitrogen abundance.

BC-type supergiants are rare and so we resort to an abundance analysis of the Galactic BC0.7 Ia HD 2905 (Lennon et al. 1993), using identical techniques to those employed for the present sample. Photometric and distance information was taken from Humphreys (1978), i.e., $V = 4.16, B - V = 0.14$ with a distance modulus of 10.2 mag (i.e., 1.1 kpc) appropriate for Cas OB14. Observational data are drawn from Smartt et al. (2002) for which HD 2905 served as a Galactic early B abundance standard. The absolute visual magnitude of $M_{\rm V} = -7.4$ mag follows from the final model intrinsic colour, $(B - V)_0 = -0.27$.

In the absence of *FUSE* far-UV spectroscopy for HD 2905, we adopt $v_\infty = 1105$ kms^{-1} for our analysis, plus $v \sin i$=91 kms^{-1} (Howarth et al. 1997). Our derived parameters for HD 2905 are given in Table 5 together with recent non-LTE results by Kudritzki et al. (1999) and Smartt et al. (2002). Comparisons between the final model and the observed spectrum are shown in Figure 12. For consistency with the other early B-type supergiants in our sample we adopted a microturbulence of $\xi = 20$kms^{-1}. This value gives excellent agreement for the He I/II and Si III lines however, as also seen in AV 70 and 372, the predicted intensity

of the Si IV λ4116 line is too strong.

Our derived temperature, $T_{\rm eff}$= 22.5 kK, is 1000-1500 K lower than found by Kudritzki et al. or Smartt et al. The former study merely adopted the appropriate Si IV/Si III temperature scale from the McErlean et al. (1999) non-LTE unblanketed, plane-parallel work, whilst an equivalent analysis was carried out by Smartt et al. (2002). Using the approximate methods of Puls et al. (1996), the mass-loss rate determined for HD 2905 by Kudritzki et al. (1999) is in reasonable agreement with the present study.

The diagnostic nitrogen lines (i.e., N II λ4601–43, 3995) are well matched by a 1.3 times Solar abundance of log(N/H)+12=8.15. The numerous O II features are best fit with an approximately Solar oxygen abundance of log(O/H)+12=8.7, which closely matches the region in the vicinity of λ4650. Carbon is more problematic, such that we tentatively adopt a 1/5 Solar abundance of log(C/H)+12$\sim$8 from C II λ4267.

Therefore, HD 2905 reveals marginally processed CNO abundances. Assuming it was formed from moderately sub-solar ISM material, carbon has been slightly reduced with nitrogen showing a modest enrichment, and oxygen unaffected. It would certainly be of interest to revisit further Galactic targets, e.g., those studied by Massa et al. (1991). They found evidence of significant nitrogen enhancement in the Galactic BN1 star HD 93840, yet solar abundances for the normal comparison star, ζ Per. Their results for the morphologically normal star are not necessarily at odds with our values for HD 2905 since both of their targets are less luminous type-Ib supergiants, for which mass-loss may have had less impact on the appearance of the atmospheres.

From our analysis of HD 2095 we take greater confidence in our present results, such that the general nitrogen enrichment versus the Magellanic Cloud ISM abundances appears to be genuine. For comparison, Smartt et al. obtained significantly smaller values (over a factor of five) using non-LTE, plane-parallel (unblanketed) models for their analysis. This indicates the degree of uncertainty in the absolute abundance ratios for B supergiant analyses when different techniques are used.

The implications of the inclusion of rotation on surface abundances from theoretical evolutionary models are well documented e.g., Meynet (1998), Heger & Langer (2000) and Maeder & Meynet (2001). Qualitative evidence of rotationally-induced mixing was given by Howarth & Smith (2001) who found that ON-type main sequence stars were drawn from a more rapidly rotating population than those with morphologically normal spectra. More recently, the enhanced nitrogen abundances found in Paper I and in AV 83 (Hillier et al, 2003) were attributed to rotational mixing, in combination with the effects of CNO processing.

We obtain significantly enhanced nitrogen abundances for all of our targets. When

compared to the abundances from Rusell & Dopita (1992), the N/C ratios for the current sample represent enhancements by factors of about 100. Enhanced nitrogen abundances were found by Maeder & Meynet (2001) in their high-mass, fast-rotating ($v\sin i = 300\,\mathrm{kms}^{-1}$) models, however it seems unlikely that our results are solely attributable to rapid rotation. Indeed if high rotational velocities were implicated, our targets would have "spun down" more quickly than the Maeder & Meynet models (see their Table 1). A more plausible solution is that rotational mixing is more effective than previously thought, even at relatively moderate velocities (as also concluded by Trundle et al. 2004).

In Table 4 we also include abundances derived for the nebula of the luminous blue variable (LBV) R127 in the LMC. It is clear that the stellar enrichment as indicated by N/O of some OB supergiants actually exceed those of the LBV nebula.

7. Temperature calibrations for OB supergiants

Several recent studies have indicated that commonly adopted temperatures for O-type stars were too high. Martins et al. (2002) used line-blanketed, spherical models for Galactic O-type dwarfs to indicate a modest downward revision, whilst a substantial downward revision was indicated for extreme O-type supergiants in Paper I using similar techniques. In their analyses of Galactic O-type stars both Herrero et al. (2002) and Bianchi & Garcia (2002) also found lower temperatures than from previous studies (although the methods of Bianchi & Garcia differ in that they rely solely on the UV-region, neglecting the traditional optical lines). Such downward revisions of temperatures (of order 10-20%) are commensurate with the initial line-blanketed results of Hubeny et al. (1998) for 10 Lac.

Our derived temperatures are plotted as a function of spectral type in Figure 13, together with the widely used Schmidt-Kaler (1982) calibration and that of Dufton et al. (2000), which represents the recently adopted late O and early B-type calibration based on unblanketed TLUSTY models (McErlean et al. 1999). This neatly illustrates the effect played by blanketing and stellar winds when compared to the unblanketed temperatures; in general we find differences of $\sim$2 kK. However, AV 488 deviates from this general trend in the sense that it lies perfectly on the unblanketed results. This result is consistent with the temperatures found from recent line-blanketed, non-LTE analyses of early B-type SMC supergiants by Trundle et al. (2004). As Table 6 indicates, temperatures of stars with strong winds (Hα in emission), deviate more from standard (plane-parallel) calibrations than those with weak winds (Hα in absorption) such as AV 488, as might be anticipated.

Published temperature calibrations have always been monotonic in nature, i.e., $T_{\rm eff}$ de-

creases with later spectral types, (e.g., Vacca et al. 1996), but this is only the case when one separates extreme supergiants (typically Ia$^+$ luminosity class) from normal supergiants (typically Ib, II). Therefore, considering the Hα model for the extreme B0 Ia supergiant AV 235 together with AV 488 (B0.5 Ia), it is the high wind density of the former and low wind density of the latter which conspire to upset the conventional downward sequence. The peculiarity of this situation is reduced when considering the Hγ model; a hotter temperature is required to match the optical spectrum when a lower wind density (i.e., smaller mass-loss rate) is required. Similar arguments have already been made recently by Herrero et al. (2002).

Further work on a yet larger Magellanic Cloud sample including *FUSE* and UVES observations, spanning early-type dwarfs and later B-type supergiants is ongoing and should further elucidate the temperature scale for early-type stars. Similarly, a larger study of Galactic early B supergiants is currently in progress which confirms the present temperature scale for B supergiants with or without strong winds (Crowther et al. 2004, in preparation).

8. Wind density and momentum

The wind-momentum-luminosity relationship (WLR, Puls et al. 1996), relating $\dot{M}$, v_∞ and $(R_*/R_\odot)^{0.5}$ to stellar luminosity has been claimed to provide a means by which distances to galaxies containing OBA-type supergiants may be obtained (e.g., Kudritzki et al. 1999). Indeed, in external galaxies B-type supergiants are generally considered to be more useful than O-types as they are visually brighter. There are two direct consequences of the present results (together with those from Paper I) regarding the calibration of the WLR. Firstly, as a direct consequence of lower temperatures from our blanketed model atmospheres, derived luminosities are lower (recall Figure 19 from Paper I). Also, given the indications that OB-type winds are clumped, there will be a second correction to the absolute value of the wind-momentum. Unfortunately, determining clumping factors remains a formidable challenge.

Kudritzki et al. (1999) discuss differences in wind driving lines between O, B and A-type supergiants, such that each will possess different scaling laws (see also Kudritzki & Puls 2000). We therefore present our current (unclumped) results in Figure 14 together with calibrations from (unblanketed) models of Galactic OB-type supergiants obtained by Kudritzki & Puls. We present two values for AV 235 given the contradictory mass-loss diagnostics for this particular star. Herrero et al. (2002) provide an updated calibration for Galactic O-type supergiants using blanketed model results, with a similar slope to Kudritzki & Puls for high luminosities, but $\sim$0.2 dex lower for moderate luminosities.

The Magellanic Cloud stars from our present sample generally lie within a factor of two of the Kudritzki & Puls calibration, in spite of the lower luminosities as a result of blanketing and (predicted) weaker winds as a result of lower metallicity. At first glance this is rather puzzling. However, we include in our sample the most extreme OB-type supergiants in the Magellanic Clouds, such that they will provide rather poor templates with which Galactic supergiants should be compared. Consequently, firm results will only be possible once large numbers of O and B-type stars have been studied in the Milky Way, LMC and SMC. Work towards this goal is presently underway by various groups. Clumping, with volume filling factors of order 10%, in which mass-loss rates are actually a factor of three times lower, would serve to reduce the calibration by 0.5 dex.

The (unclumped) mass-loss rates for our sample are compared with the theoretical predictions for our stars from the recipes of Vink et al. (2001) in Figure 15; since the methods are identical, results from Paper I and Hillier et al. (2003; using the unclumped $\dot{M}$ for AV 83) are also included. In the figure the open symbols are the theoretical mass-loss rates calculated for $(Z/Z_{\odot}) = 1$. The solid symbols are the theoretical mass-loss rates calculated for the appropriate metallicity, i.e., $(Z/Z_{\odot}) = 0.2$ or 0.4; the diagonal dotted line simply indicates the 1:1 relationship. The plot is somewhat complicated by the fact for some stars there is not a constant offset between points for the same star at the two metallicities. This arises because some of our stars (most notably AV 235, with the lowest predicted mass-loss rate) lie between the two bi-stability jumps. In these cases the jump is recalculated by Vink's routine, which due to the metallicity dependence (see Vink et al., Eqn. 15), leads to different coefficients when calculating the predicted rates; similar problems were encountered by Trundle et al. (2004).

The first point to note from the figure is that the observationally derived mass-loss rates are generally higher for our LMC stars than those in the SMC; this is simply a selection effect of the current overall sample. Four of the five LMC stars are classified as Ia^{+}, whereas the SMC stars are generally less extreme. This is unfortunate as it makes it difficult to perform meaningful comparisons between the two metallicities. A second comment is that the theoretical results at $(Z/Z_{\odot}) = 1$ (i.e., assuming no Z dependence) are qualitatively a better match to the observed mass-loss rates than those taking metallicity into account. Similarly, for three early B-type supergiants in the SMC, Trundle et al. (2004) also found that the observationally derived mass-loss rates were larger than those predicted for $(Z/Z_{\odot}) = 0.2$. Vink et al. used different sets of stellar atmosphere models and thus no physical significance should be attached to these results at the current time. They do however reinforce the need for further theoretical efforts in the sense that the "recipe" to predict stellar-mass loss rates gives different values to the analyses here and to those by Trundle et al. (2004). Similarly, if one is to reliably test the dependence of stellar mass-loss rates with metallicity, it is clear

that we require a large, *homogenous* observational study of early-type stars in the Clouds.

9. Conclusions

We have studied a sample of LMC and SMC late O and early B supergiants based on modern line-blanketed, spherical models plus extensive *FUSE* (far-UV), *IUE* (UV) and UVES (visual) observations. In general, we find excellent agreement between alternative optical temperature diagnostics (e.g., He and Si) with Hα derived mass-loss rates. Adopting homogeneous models, some UV wind features are systematically too strong.

The UV discrepancies are reduced if OB winds are clumped. P V $\lambda\lambda$1118-1128 was identified as a useful probe of clumping in O supergiants in Paper I, unless phosphorus is depleted relative to other elements in the Magellanic Clouds. In the present study, S IV $\lambda\lambda$1063-1072 appears to offer an equivalent probe in early B-type supergiants, with the additional benefit that the ISM sulphur abundance is well known (Russell & Dopita 1992). We conclude that winds in OB-type stars are at least moderately clumped. This leads to lower derived mass-loss rates than otherwise, which scale with the adopted filling-factor, (with $f_\infty = 0.1$, $\dot{M}$ is reduced by a factor of $\sim$3). AV 235 (B0 Iaw) is peculiar in the current sample in that it has inconsistent optical (Balmer line), UV and far-UV wind features. All diagnostics indicate a relatively weak (and clumped) wind for AV 235 with the exception of Hα.

Stellar temperatures for O and early B-type supergiants are generally 2–4 kK lower than recent calibrations based on unblanketed, plane-parallel models. Supergiants with extreme (typically Ia$^+$) winds are more greatly affected, such that there is expected to be different spectral type–temperature calibrations for OB supergiants, depending on whether Hα is in emission. Reduced temperatures consequently indicate lower luminosities, with impact upon ionizing fluxes (recall Figure 13 from Herrero et al. 2002), and wind-momentum luminosity calibrations.

We also investigate CNO abundances for OB supergiants. As in Paper I, "normal" OB supergiants are found to have partially processed abundances, i.e., log(N/C)$\sim$1 versus log(N/C)~ -1 for H II regions. Although such large nitrogen enrichments were found in the fast-rotating evolutionary models from Maeder & Meynet (2001), it seems unlikely that rapid rotation is solely responsible and that mixing is perhaps more effective than previously thought at more moderate velocities. A differential analysis of HDE 269896 (ON9.7 Ia$^+$) versus Sk-66°169 (O9.7 Ia$^+$) indicates even more extreme abundances – nitrogen is further enriched at the expense of carbon and oxygen in the ON supergiant. In contrast, two OBC

stars exhibit fairly normal CNO abundances; HD 2905 studied here for comparison to the Magellanic Cloud B-type supergiants, plus AV 69 investigated by Hillier et al. (2003) using identical techniques. Consequently, quantitative models now provide strong evidence for the sequence OBC (normal CNO) $\longrightarrow$ OB (CNO partially processed) $\longrightarrow$ OBN (fully CNO processed) originally suggested on from morphological arguments by Walborn (1976, 1988) and supported by studies of He-contents by Smith & Howarth (1994).

10. Acknowledgements

Financial support has been provided by PPARC (CJE), the Royal Society (PAC). JDH acknowledges support from NASA grants NAGW-3828 and NAG5-10377 and NASA Space Telescope Science Institute (STScI) grant AR07985.02-96A. We thank Lex Kaper for providing his UVES data, Thierry Lanz for supplying a TLUSTY B-supergiant model, Stephen Smartt for kindly providing the HD2905 data and Jay Abbott for reducing the ANU data.

REFERENCES

Asplund M., 2003, in CNO in the Universe, eds. C. Charbonnel, D. Schaerer, G. Meynet, ASP Conf. Series 304, San Francisco, p279

Ardeberg A., Brunet J.-P., Maurice E., Prévot L., 1972, A&AS, 6, 249

Azzopardi M., Vigneau J., 1975, A&AS, 22, 285

Bianchi L., Garcia M., 2002, ApJ, 581, 610

Bouret J-C., Lanz T., Hillier, D. J. et al, 2003, ApJ, 585, 1182

Busche, 2001, Ph.D. thesis, Univ of Pittsburgh

Busche, Hillier D. J., 2004, AJ, submitted

Crowther P. A., Hillier D. J., Evans C. J. et al., 2002, ApJ, 579, 774 (Paper I)

Dachs J., 1970, A&A, 9, 95

Dufton P. L., McErlean N. D., Lennon D. J., Ryans R. S. I., 2000, A&A, 353, 311

Ehrenfreund P., Cami J., Jiménez-Vicente J. et al., 2002, ApJ, 576, 117L

Evans C. J., Howarth I. D., Irwin M. J. et al., 2004, MNRAS, in press

Eversberg T., Lepine S., Moffat A. F. J., 1998, ApJ, 494, 799

Fitzgerald M. P., 1970, A&A, 4, 234

Fitzpatrick E. L., 1985, ApJS, 59, 77

Fitzpatrick E. L., 1991, PASP, 103, 1123

Fullerton A. W., Crowther P. A., De Marco O. et al., 2000, ApJ, 538, 43L

Haser S. M., 1995, Ph.D. thesis, University of Munich

Grevesse N., Sauval A.J., 1998, Space Sci Rev. 85, 161

Heger A., Langer N., 2000, ApJ, 544, 1016

Herrero A., Kudritzki R-P., Vilchez J. M. et al., 1992, A&A, 261, 209

Herrero A., Puls J., Najarro F., 2002, A&A, 396, 949

Hillier D. J., 1991, A&A, 247, 455

Hillier D. J., Miller, D. L., 1998, ApJ, 496, 407

Hillier D. J., Lanz T., Heap S. R. et al., 2003, ApJ 588, 1039

Howarth I. D., Siebert K. W., Hussain G. A. J., Prinja R. K., 1997, MNRAS, 284, 265

Howarth I. D., Smith K. C., 2001, MNRAS, 327, 353

Hubeny I., Heap S. R., Lanz, T., 1998, in Howarth I. D., ed., Boulder-Munich II: Properties of Hot, Luminous Stars, ASP Conf. Series 131, San Francisco, p. 108

Humphreys R. M., 1978, ApJS, 38, 309

Humphreys R. M., McElroy, D. B., 1984, ApJ, 284, 565

Kudritzki R-P., Pauldrach A., Puls J., 1987, A&A, 173, 293

Kudritzki R-P., Puls J., Lennon D. J. et al., 1999, A&A, 350, 970

Kudritzki R-P., Puls, J., 2000, ARA&A, 38, 613

Leitherer C., Leão J. R. S., Heckman T. M. et al., 2001, ApJ, 500, 724

Lennon D. J., Kudritzki R-P., Becker S. T. et al, 1991, A&A, 252, 498

Lennon D. J., Dufton P. L., Fitzsimmons A., 1993, A&AS, 94, 569

Maeder A., Meynet G., 2001, A&A, 373, 555

Martins F., Schaerer D., Hillier D. J., 2002, A&A, 382, 999

Massa D., 1989, A&A, 224, 131

Massa D., Altner B., Lamers H. J. G. L. M., 1991, A&A 242, 188

Massa D., Fullerton A. W., Nichols J. S. et al., 1995, ApJ, 452, L53

Massa D., Fullerton A. W., Sonneborn G., Hutchings J. B., 2003, ApJ, 586, 996

Massey P., Lang C. C., DeGioia-Eastwood K., Garmany C. D., 1995, ApJ, 438, 188

Massey P., 2002, ApJS, 141, 81

McErlean N.D., Lennon D.J., Dufton P. L., 1999, A&A 349, 553

Meynet G., 1998, in Howarth I. D., ed., Boulder-Munich II: Properties of Hot, Luminous Stars, ASP Conf. Series 131, San Francisco, p. 96

Miller N. A., Cassinelli J. P., Waldron W. L. et al, 2002, ApJ, 577, 951

Moffat A. F. J., Drissen L., Lamontagne R., Robert C., 1988, ApJ, 334, 1038

Moos H. W., Cash W. C., Cowie L. L. et al., 2000, ApJ, 538, L1

Nandy K., Morgan D. H., Houziaux L., 1990, MNRAS, 245, 318

Owocki S. P., Castor J. I., Rybicki G. B., 1988, ApJ, 335, 914

Pellerin A., Fullerton A. W., Robert C. et al., 2002, ApJS, 143, 159

Prinja R. K., Barlow M. J., Howarth I. D., 1990, ApJ, 361, 607

Prinja R. K., Crowther P. A., 1998, MNRAS, 300, 828

Prinja R. K., Massa D., Fullerton A. W., 2002, A&A, 388, 587

Puls J., Kudritzki R-P., Herrero A. et al., 1996, A&A, 305, 171

Rolleston W.R.J., Venn K., Tolstoy E., Dufton P.L., 2003, A&A 400, 21

Russell S. C., Dopita M. A., 1992, ApJ, 384, 508

Schmidt-Kaler T., 1982, in Schaifers K., Voigt H. H., eds., Landolt-Börnstein, Group VI, Vol 2b, Springer-Verlag, p. 1

Slettebak A., 1988, PASP, 100, 770

Smartt S. J., Lennon D. J., Kudritzki R-P. et al., 2002, A&A, 391, 979

Smith K. C., Howarth I. D., 1994, A&A, 290, 868

Smith L. J., Nota A., Pasquali A. et al, 1998, ApJ, 503, 278

Trundle C., Lennon D. J., Puls J., Dufton P. L., 2004, A&A, in press

Tumlinson J.,. Schull J. M., Rachford B. L. et al., 2002, ApJ, 566, 857

Vacca W. D., Garmany C. D., Shull J. M., 1996, ApJ, 460, 914

Venn K. A., 1999, ApJ, 518, 405

Villamariz M. R., Herrero A., Becker S. R., Butler K., 2002, A&A, 388, 940

Vink J. S., de Koter, A., Lamers H. J., 2001, A&A, 369, 574

Vrancken M., Lennon D. J., Dufton P. L., Lambert D. L., 2000, A&A, 358, 639

Walborn N. R., 1976, ApJ, 205, 419

Walborn N. R., 1977, ApJ, 215, 53

Walborn N. R., 1983, ApJ, 265, 716

Walborn N.R., 1988, in Nomoto K., ed., Proc IAU Coll 108: Atmospheric Diagnostics of Stellar Evolution, Springer, Berlin, p. 70

Walborn N. R., Fitzpatrick E. L., 1990, PASP, 102, 379

Walborn N. R., Lennon D. J., Haser S. M. et al., 1995, PASP, 107, 104

Walborn N. R., Parker J. W., Nichols J. S., 1995, *International Ultraviolet Explorer* Atlas of B-type Spectra from 1200 to 1900Å (NASA RP1363; Washington

Walborn N. R., Howarth I. D., 2000, PASP, 112, 1446

Walborn N. R., Fullerton A. W., Crowther P. A. et al., 2002, ApJS, 141, 443

Table 1. Observational parameters of target stars

Star	Alias	Galaxy	Sp. Type	Ref.	V mag	$B-V$ mag	Ref.	$E(B-V)$ mag	M_V mag	v_r [kms^{-1}]	log N(H I) [cm^{-2}]	log N(H_2) [cm^{-2}]
AV 469	Sk 148	SMC	O8.5 II((f))	7	13.20	−0.22	2	0.09	−6.0	187	21.3	–
AV 372	Sk 116	SMC	O9 Iabw	7	12.59	−0.15	4	0.12	−6.7	262	21.8	16.5
AV 70	Sk 35	SMC	O9.5 Ibw	6	12.38	−0.17	2	0.10	−6.8	170	21.3	–
AV 456	Sk 143	SMC	O9.5 Ibw	8	12.83	0.10	4	0.35	−7.2	169	–	–
HDE 269896	Sk-68°135	LMC	ON9.7 Ia$^+$	5	11.36	0.00	1	0.25	−7.9	290	21.5	19.9
HDE 269050	Sk-68°52	LMC	B0 Ia	5	11.54	−0.07	1	0.17	−7.5	234	21.6	19.5
AV 235	Sk 82	SMC	B0 Iaw	5	12.20	−0.18	2	0.07	−6.9	161	21.3	15.9
AV 488	Sk 159	SMC	B0.5 Iaw	6	11.90	−0.13	3	0.09	−7.3	200	18.9	18.9

Note. — Reddenings and absolute magnitudes were derived from the mean of intrinsic colours from Fitzgerald (1970) and from fitting stellar models to UV-optical spectrophotometry. Neutral hydrogen column densities for our targets (with the exception of AV 456) are determined from fits to the wings of the Lyman β line in the *FUSE* spectra. Molecular hydrogen column densities from Tumlinson et al. (2002) are also given where available.

References. — (1) Ardeberg et al. (1972), (2) Azzopardi & Vigneau (1975), (3) Dachs (1970), (4) Massey (2002), (5) Walborn (1977), (6) Walborn (1983), (7) Walborn et al. (2002), (8) this work.

Table 2. Details of VLT-UVES, *FUSE* and other UV observations of target stars

Star	*FUSE* ID	Exp. [min]		Date		Optical coverage [Å]	Archival data	*IUE* Image
		FUSE	VLT	*FUSE*	VLT			
AV 469	P1176301	136	33	2000/10/11	2001/09/27	3770–4945, 6380–8200	*HST*-FOS	–
AV 372	P1176501	73	40	2000/10/11	2001/09/27	3770–4945, 6380–8200	*HST*-FOS	–
AV 70	B0900601	103	28	2001/06/15	2001/09/24	3400–5750, 5830–6800	*IUE*-LORES	SWP18830
AV 456	Q1070101	62	30	2000/10/11	2001/09/24	3400–4500, 4670–6650	*IUE*-LORES	SWP45199
HDE 269896	P1173901	118	29	2000/02/12	2001/09/24	3400–5750, 5830–8310	*IUE*-HIRES	SWP47594
HDE 269050	P1174001	135	20	2000/10/01	2001/09/29	3770–4945, 6380–8200	*IUE*-HIRES	SWP53054
AV 235	P1030301	270	17	2000/07/02	2000/09/27	3770–4945, 6380–8200	*IUE*-HIRES	SWP13535
AV 488	P1030501	113	28	2000/10/04	2001/09/24	3400–5750, 5830–8510	*IUE*-HIRES	SWP16614

Table 3. Derived parameters of target stars

Star	Sp. Type	$T_{\rm eff}$[a] [kK]	R_* [$R_\odot$]	log$g$ [cgs]	log($L/L_\odot$)	$\dot{M}$ [$M_\odot$ yr^{-1}]	f	β	v_∞ [kms^{-1}]	$v$sin$i$ [kms^{-1}]
AV 469	O8.5 II((f))	33.0	17.2	3.4	5.50	1.3×10^{-6}	1.0	1.00	1550	80
						5.0×10^{-7}	0.1			
AV 372	O9 Iabw	28.0	27.5	3.1	5.62	1.0×10^{-6}	1.0	2.25	1550	120
						3.5×10^{-7}	0.1	2.75		
AV 70	O9.5 Ibw	28.5	28.4	3.1	5.68	1.5×10^{-6}	1.0	1.75	1450	100
						4.5×10^{-7}	0.1			
AV 456	O9.5 Ibw	29.5	30.6	3.0	5.81	7.0×10^{-7}	1.0	1.75	1450	80
		30.5	28.6			3.0×10^{-7}	0.1			
HDE 269896	ON9.7 Ia$^+$	27.5	42.3	2.7	5.97	7.5×10^{-6}	1.0	3.50	1350	70
						2.5×10^{-6}	0.1			
HDE 269050	B0 Ia	24.5	42.2	2.7	5.76	3.2×10^{-6}	1.0	2.75	1400	80
		25.5	39.0			9.0×10^{-7}	0.1			
AV 235 (Hα)	B0 Iaw	24.5	36.2	2.8	5.63	5.8×10^{-6}	1.0	2.50	1400	80
						1.5×10^{-6}	0.1			
AV 235 (Hγ)		27.5	31.9	2.9	5.72	4.0×10^{-6}	1.0	1.50	1400	80
						1.3×10^{-6}	0.1			
AV 488	B0.5 Iaw	27.5	32.6	2.9	5.74	1.2×10^{-6}	1.0	1.75	1250	80
						4.5×10^{-7}	0.1			

[a]As is usual for stars with extended atmospheres, stellar temperatures are defined relative to a radius of Rosseland optical depth 10.

Note. — Mass-loss rates are given for homogeneous winds (with a maximum volume filling factor f=1) and for clumped winds (f=0.1); in two instances the introduction of clumping necessitated slight changes in the other parameters to fit Hα and the other optical lines successfully. Two sets of results are given for AV 235 from fits to the Hα and Hγ lines (see §5).

Table 4. Derived CNO abundances of target stars, including those from Paper I and Hillier et al. (2003)

Star	Sp Type	ϵ(He)	log(C/H)+12	log(N/H)+12	log(O/H)+12	log (N/C)	log (N/O)	Ref
			Sun					
		0.09	8.51	7.93	8.66	−0.6	−0.7	
			LMC					
HDE 269698	O4 If$^+$	0.2:	7.3	9.1	7.8	1.8	1.3	1
HDE 270952	O6 If$^+$	0.2:	7.65	8.8	7.7	1.1	1.1	1
Sk–66°169	O9.7 Ia$^+$	0.2:	7.3	7.95	8.1	0.65	−0.15	3
HDE 269896	ON9.7 Ia$^+$	0.2	7.4	8.3	8.0	0.9	0.3	3
HDE 269050	B0 Ia	0.2	7.8	8.6	8.5	0.8	0.1	3
RD92	H II	–	8.04	7.14	8.35	−0.9	−1.21	
R127	LBV	–	–	8.05	8.10	–	−0.05	
			SMC					
AV 232	O7 If$^+$	0.2:	7.5	8.45	8.0	0.95	0.45	1
AV 83	O7 If$^+$	0.2	7.6	8.4	7.8	0.8	0.6	2
AV 69	OC7.5 III(f)	0.1	7.6	6.3	8.2	−0.7	−1.9	2
AV 469	O8.5II((f))	0.2	7.1	8.2	–	1.1	–	3
AV 372	O9 Iaw	0.15	7.3	7.8	–	0.5	–	3
AV 70	O9.5 Iaw	0.2:	7.1	8.0	<8.0	0.9	>0	3
AV 456	O9.5 Iaw	0.1	–	7.7	<8.0	–	–	3
AV 235 (Hα)	B0 Iaw	0.2	7.0	8.4	8.1	1.4	0.3	3
AV 235 (Hγ)	B0 Iaw	0.2	7.3	8.0	8.0	0.7	0.0	3
AV 488	B0.5 Iaw	0.2	7.2	8.1	8.0	0.9	0.1	3
RD92	H II	–	7.73	6.63	8.03	−1.1	−1.4	
Venn		–	7.4	6.6	8.1	−0.8	−1.5	

Note. — Also included are Solar abundances (Grevesse & Sauval 1998; Asplund 2003), Magellanic Cloud H II region abundances (Russell & Dopita 1992, Venn 1999) and that of the nebula of R127 in the LMC (Smith et al. 1998). Results from the two AV 235 models are given (see §5).

References. — (1) Paper I; (2) Hillier et al. (2003); (3) This work

Table 5. Comparison of derived parameters for HD 2905 (BC 0.7Ia) with previous studies

Parameter	K99[a]	S02[b]	This work
$T_{\rm eff}$ (kK)	24	23.5	22.5
$R_*(R_\odot)$	41		47.7
log$g$	2.7	2.7	2.7
log$(L/L_\odot)$	5.7		5.72
$\dot{M}$ $(M_\odot$ yr$^{-1})$	2.3×10^{-6}	–	2.4×10^{-6}
β	1.35	—	2
ζ (kms^{-1})	11	11	20
$v$sin$i$ (kms^{-1})		80	91[c]
$M_{\rm V}$	-7.0		-7.4
log(C/H)+12		7.0:	8.0
log(N/H)+12		7.3	8.15
log(O/H)+12		9.1	8.7

[a]Kudritzki et al. (1999)

[b]Smartt et al. (2002)

[c]Howarth et al. (1997)

Table 6. Temperature calibrations for late O and early B supergiants

Sp Type	SK82[a]	HM84[b]	L93[c]	V96[d]	D00[e]	This work	
						Hα em	Hα abs
O8.5	33.4	33.0		34.2			33.0
O9	32.6	32.6	32.0	32.7	34.0		28.0
O9.5	29.3	29.9	30.0	31.2	32.5		29.0
O9.7			27.5			27.5	
B0	26.0	28.6	25.0	28.2	28.5	24.5:	
B0.5	23.4	23.1	22.0		27.0		27.5
B0.7			21.0		25.5	22.5	
B1	20.8	20.3	20.0		23.5		

[a]Schmidt-Kaler (1982)

[b]Humphreys & McElroy (1984)

[c] Lennon et al. (1993)

[d]Vacca et al. (1996)

[e]Dufton et al. (2000)

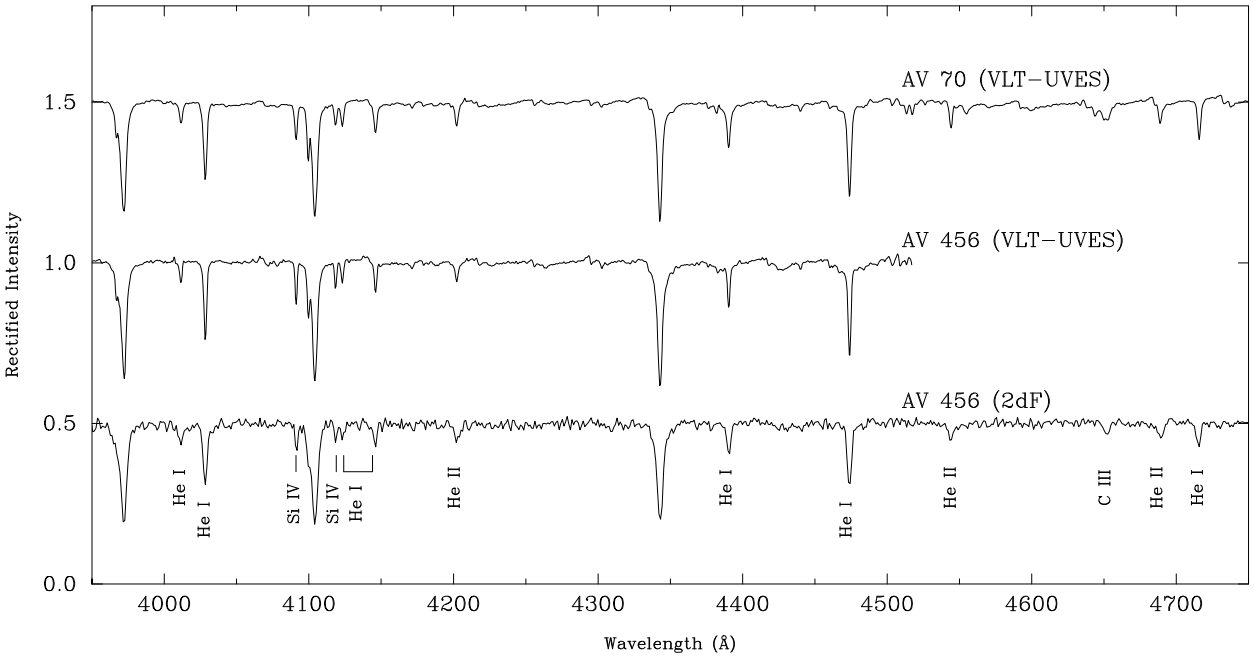

Fig. 1.— Blue-violet UVES and 2dF spectra of AV 456 compared with the UVES observation of AV 70. The features identified in the 2dF spectrum are, from left to right by ion, He I $\lambda\lambda$4009, 4026, 4121, 4144, 4388, 4471, 4713; He II $\lambda\lambda$4200, 4542, 4686; Si IV $\lambda\lambda$4089, 4116 and C III λ4650. For display purposes the UVES data have been smoothed and rebinned to a resolution of 1 Å FWHM.

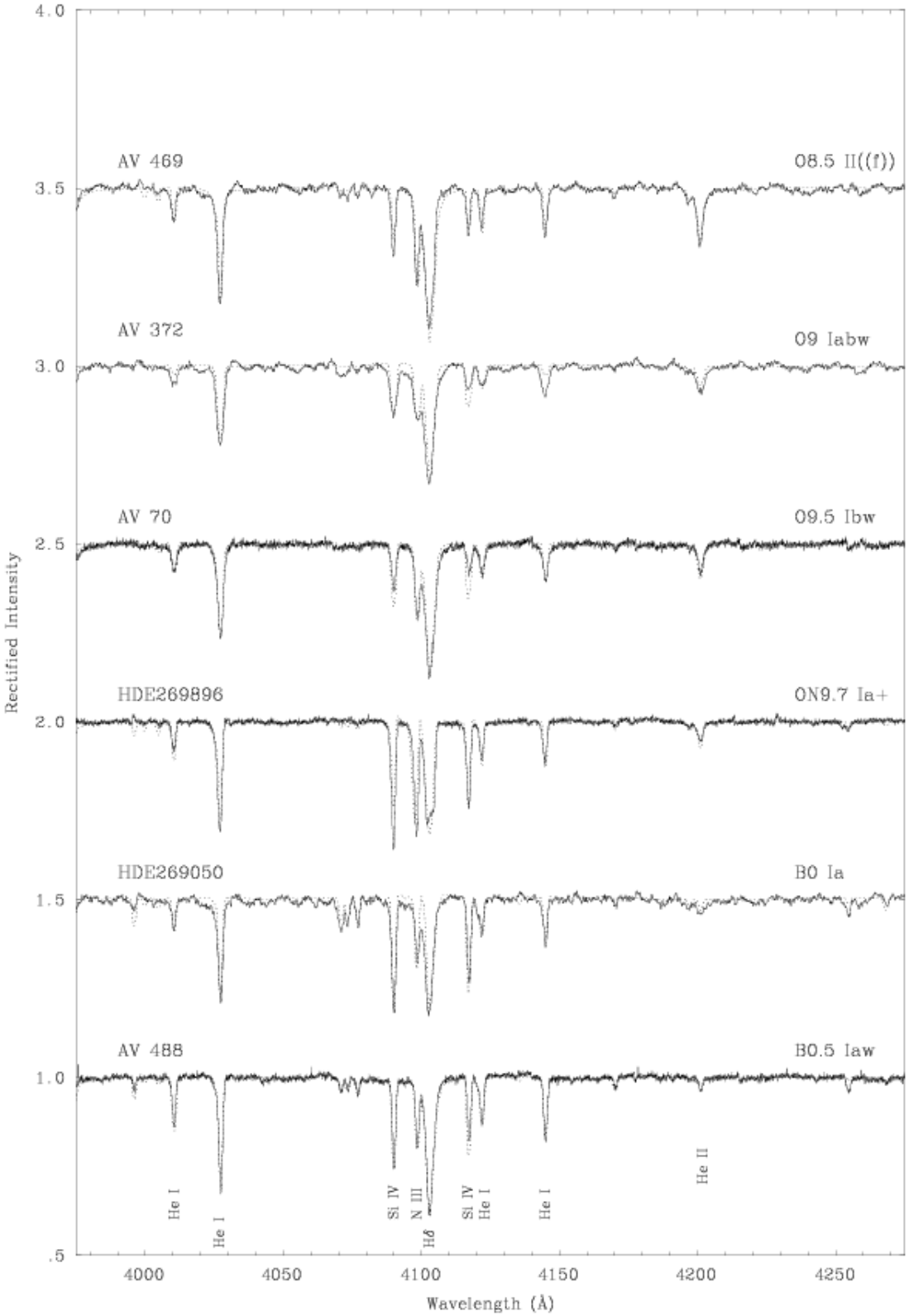

Fig. 2.— λ4000–4250 region for UVES observations (solid line) and the final homogeneous (i.e., unclumped) CMFGEN models (dotted). The lines identified are, from left to right by species, He I $\lambda\lambda$4009, 4026, 4121, 4144; He II λ4200; Si IV $\lambda\lambda$4089, 4116 N II λ3995 and N III λ4097. To aid the clarity of the comparisons (both here and in the two subsequent figures) the UVES data and model spectra have been smoothed and

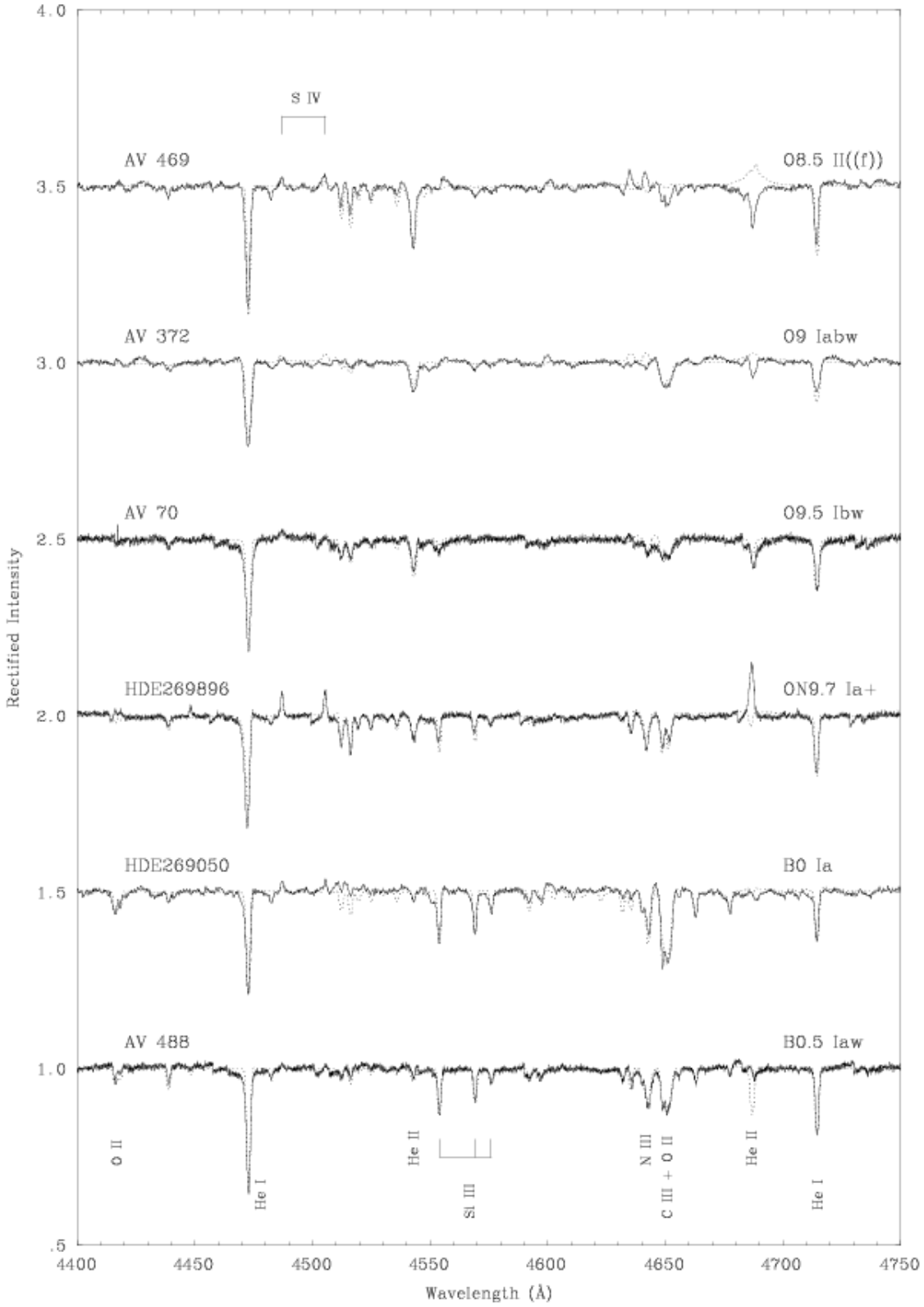

Fig. 3.— λ4450–4750 region for UVES observations (solid line) and homogeneous CMFGEN models (dotted). The lines identified in AV 488 are, from left to right, O II λ4415-17, He I λ4471, He II λ4542, Si III λ4553-68-75, N III λ4640, C III+O II λ4650, He II λ4686 and He I λ4713. The S IV $\lambda\lambda$4486-4504 emission lines are also identified in HDE 269896.

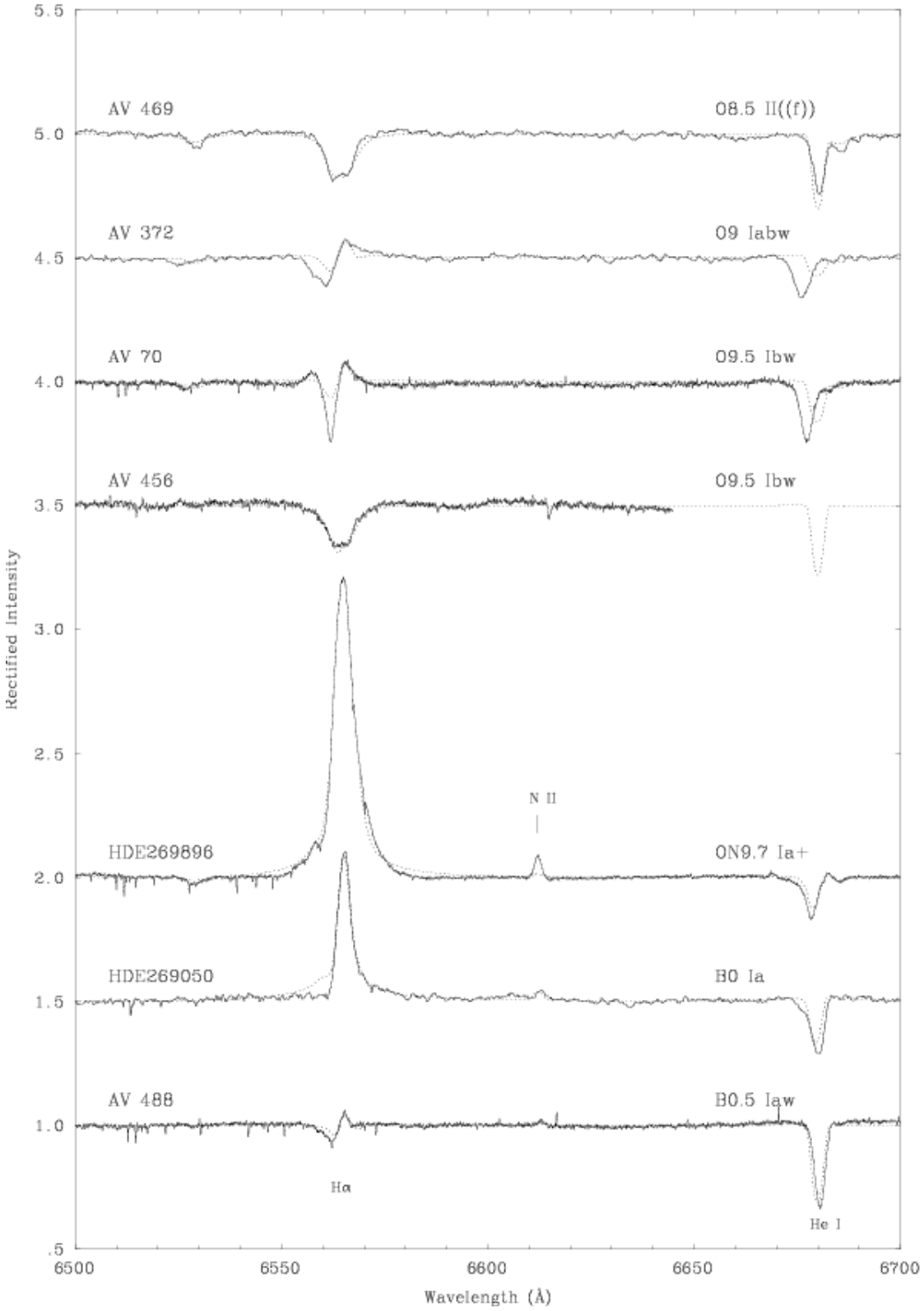

Fig. 4.— λ6500–6700 region for UVES observations (solid lines) and homogeneous CMFGEN models (dotted). The He I λ6678 line is present in each spectrum and N II λ6611 emission is seen in both HDE 269896 and 269050. The velocity offsets between the Hα and He I line are discussed in the text.

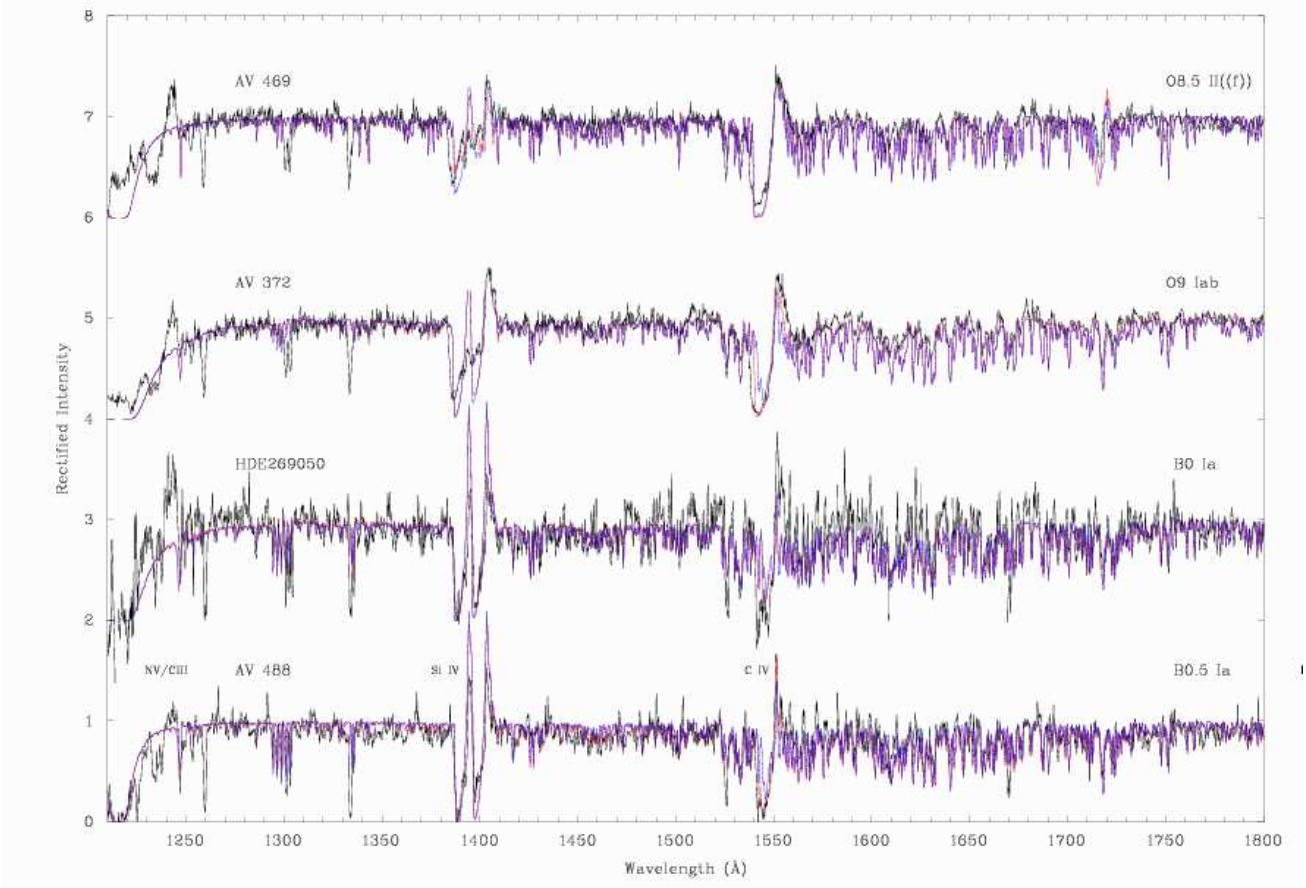

Fig. 5.— Illustrative comparison of *HST*-FOS (AV 469 & 372) and *IUE* (HDE 269050 & AV 488) data with the final CMFGEN models (unclumped – red; clumped – blue). The two lines identified in AV 488 are Si IV $\lambda\lambda$1394, 1403 and C IV $\lambda\lambda$1548-51. The model spectra were multiplied by synthetic transmission spectra to incorporate the effects of absorption by interstellar neutral hydrogen, as measured from Lyman-β (Table 1).

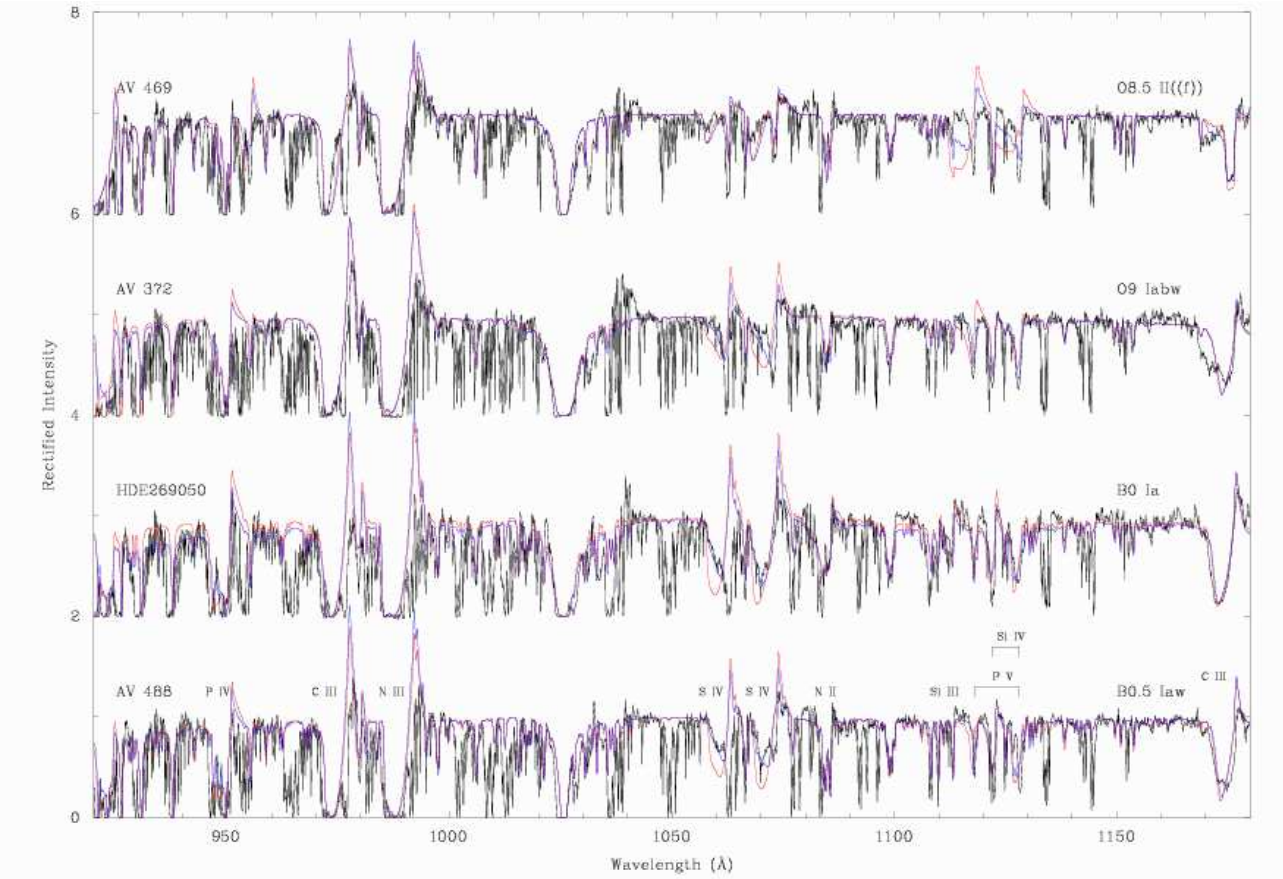

Fig. 6.— Comparison of *FUSE* data and final CMFGEN models (unclumped – red; clumped – blue). The lines identified in AV 488 are P IV λ951, C III λ977, N III λ991, S IV $\lambda\lambda$1063-73, N II λ1085, Si III$\lambda\lambda$1108-10-13, P V $\lambda\lambda$1118-28 and Si IV $\lambda\lambda$1123-28. As in Figure 5, the model spectra have been multiplied by an appropriate transmission spectrum to include the effects of absorption by interstellar neutral hydrogen.

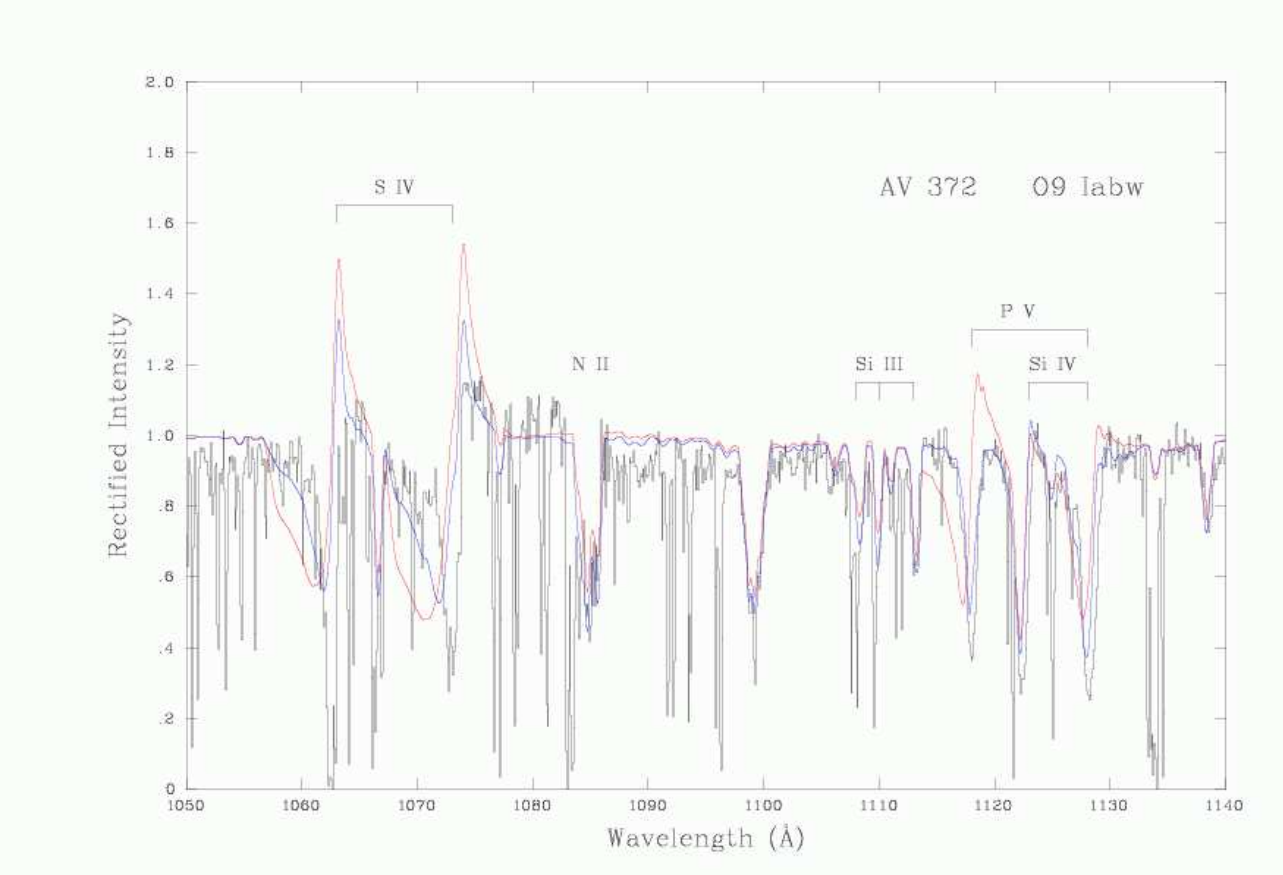

Fig. 7.— Comparison of the observed S IV $\lambda\lambda$1063-73 and P V $\lambda\lambda$1118-28 doublets with the final CMFGEN models (unclumped – red; clumped – blue) for AV 372. Additional identified lines are N II λ1085, Si III $\lambda\lambda$1108-10-13 and Si IV λ1123-28.

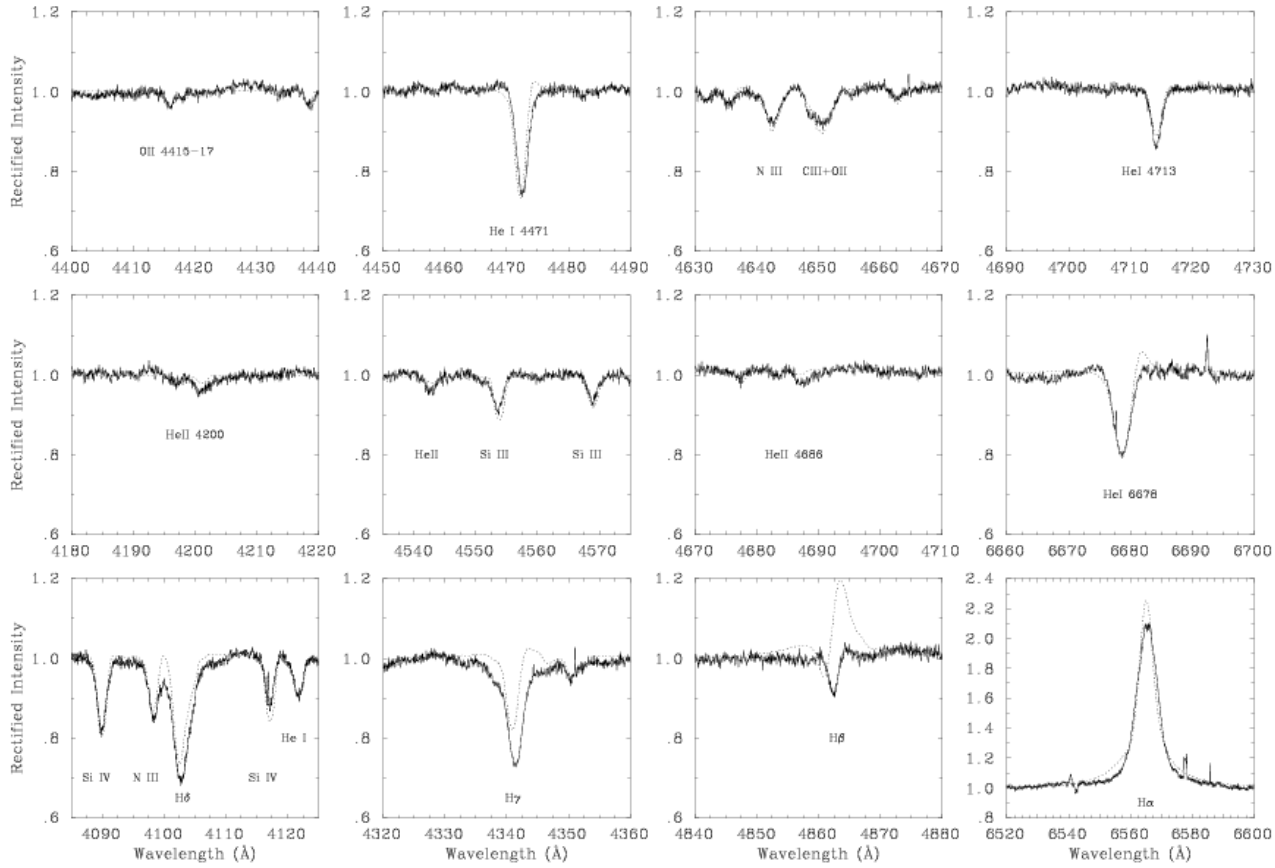

Fig. 8.— Comparison between optical UVES line profiles of AV 235 (solid line) and CMFGEN spectra (unclumped – dotted; clumped – dashed) for our Hα derived mass-loss rate.

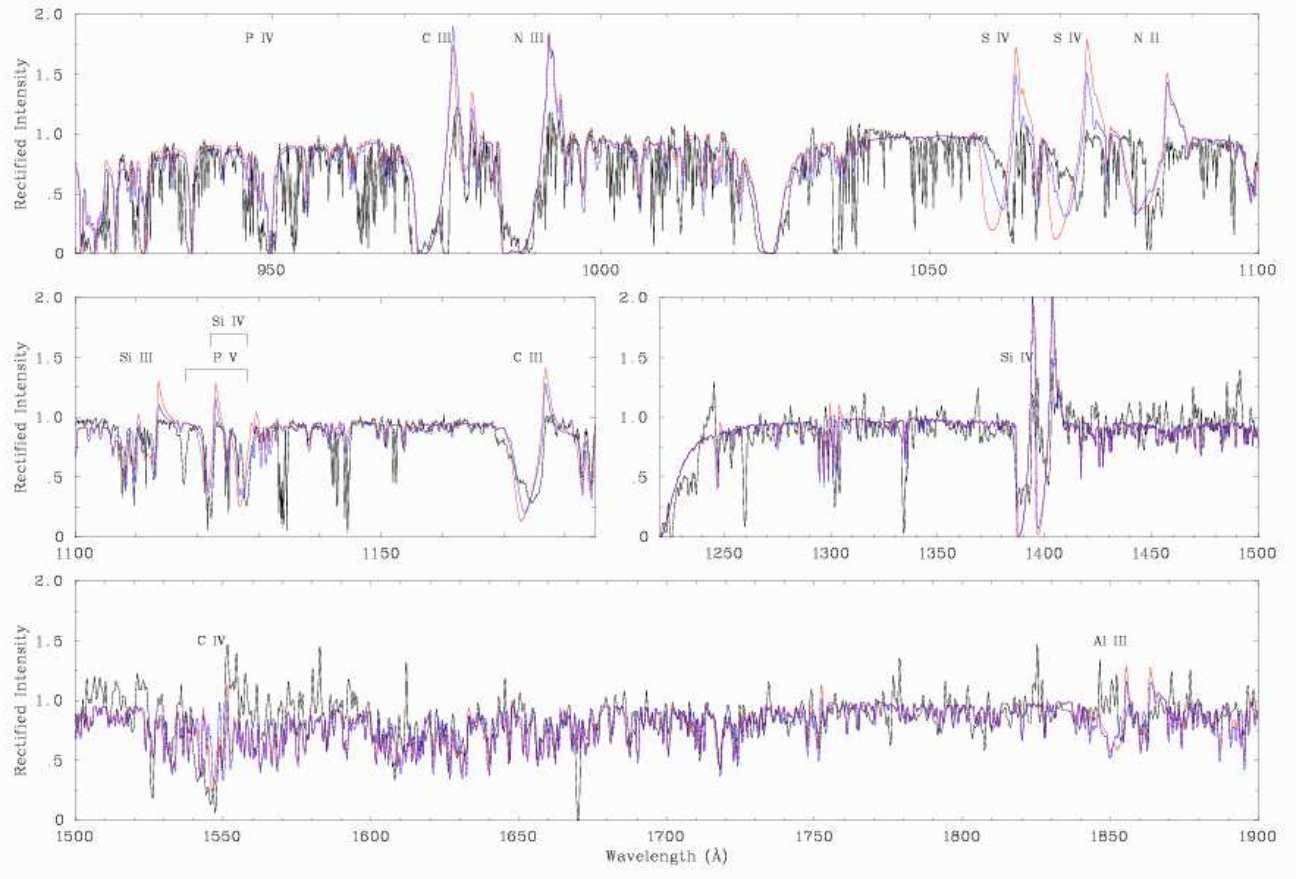

Fig. 9.— Comparison between *FUSE*/*IUE* observations of AV 235 and the Hα derived CMFGEN model spectra (unclumped – red; clumped – blue). The model spectra have been multiplied by an appropriate transmission spectrum to include the effects of neutral hydrogen absorption.

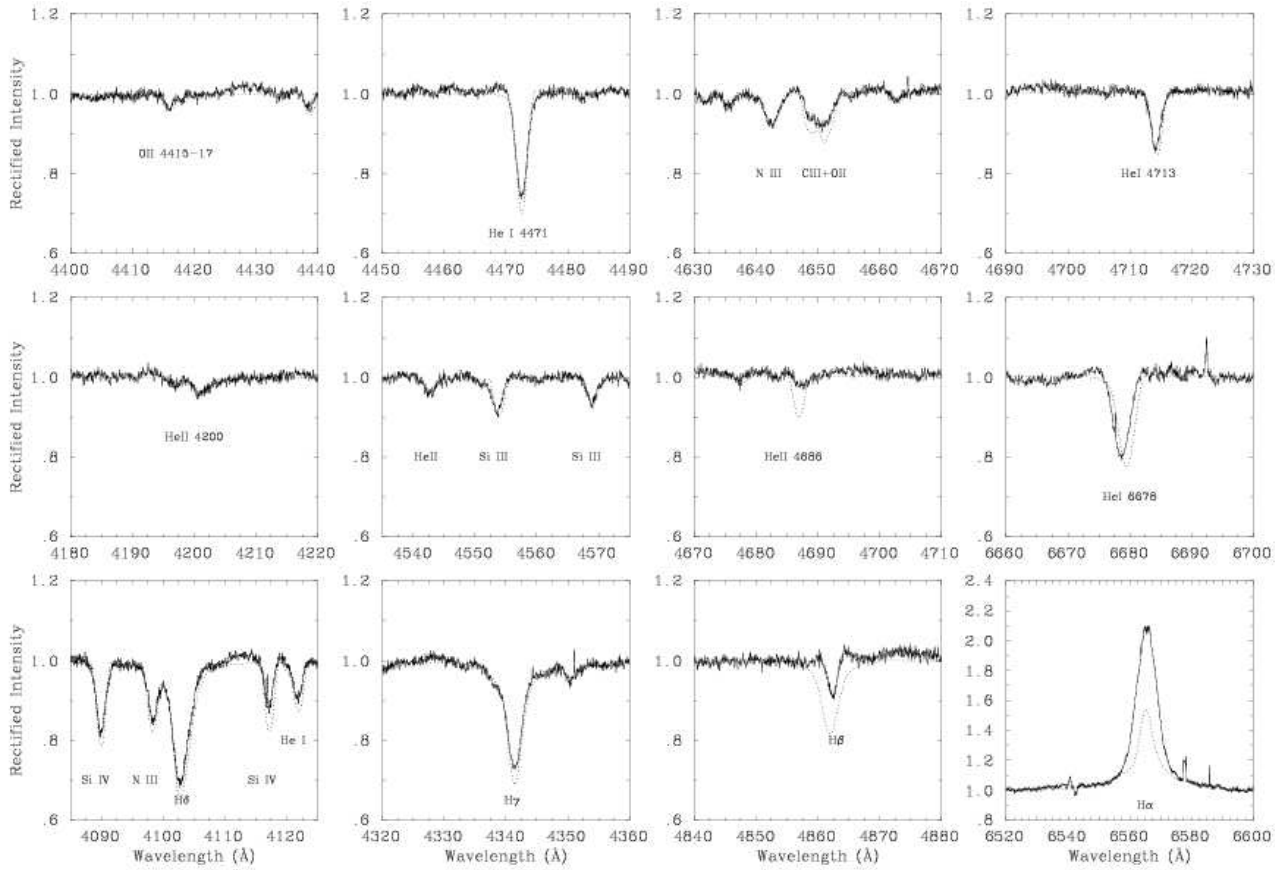

Fig. 10.— Comparison between optical UVES line profiles of AV 235 (solid line) and CMFGEN spectra (unclumped – dotted; clumped – dashed) for our Hγ derived mass-loss rate.

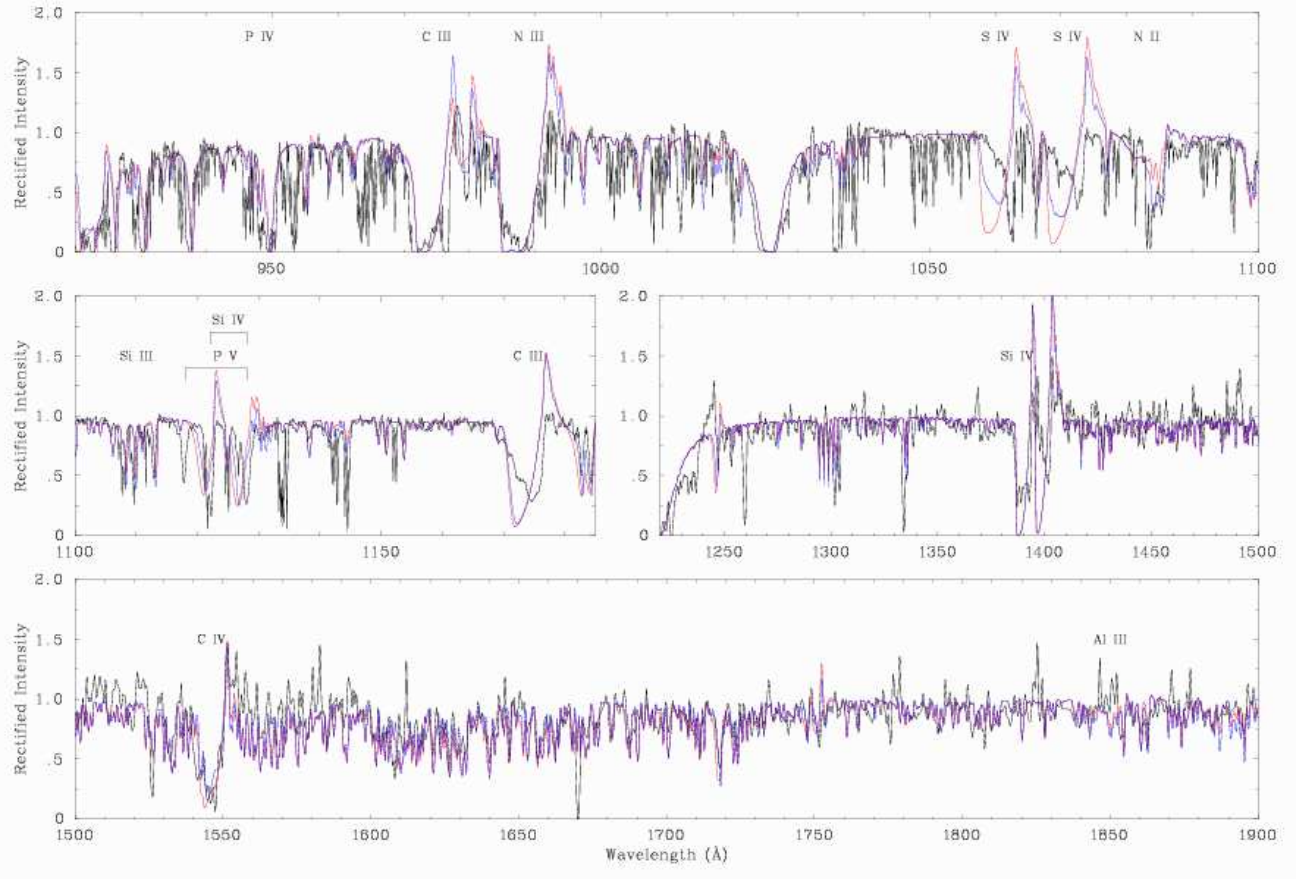

Fig. 11.— Comparison between *FUSE*/*IUE* observations of AV 235 and the Hγ derived CMFGEN model spectra (unclumped – red; clumped – blue). Again the model spectra have been multiplied by an appropriate transmission spectrum to include the effects of neutral hydrogen absorption.

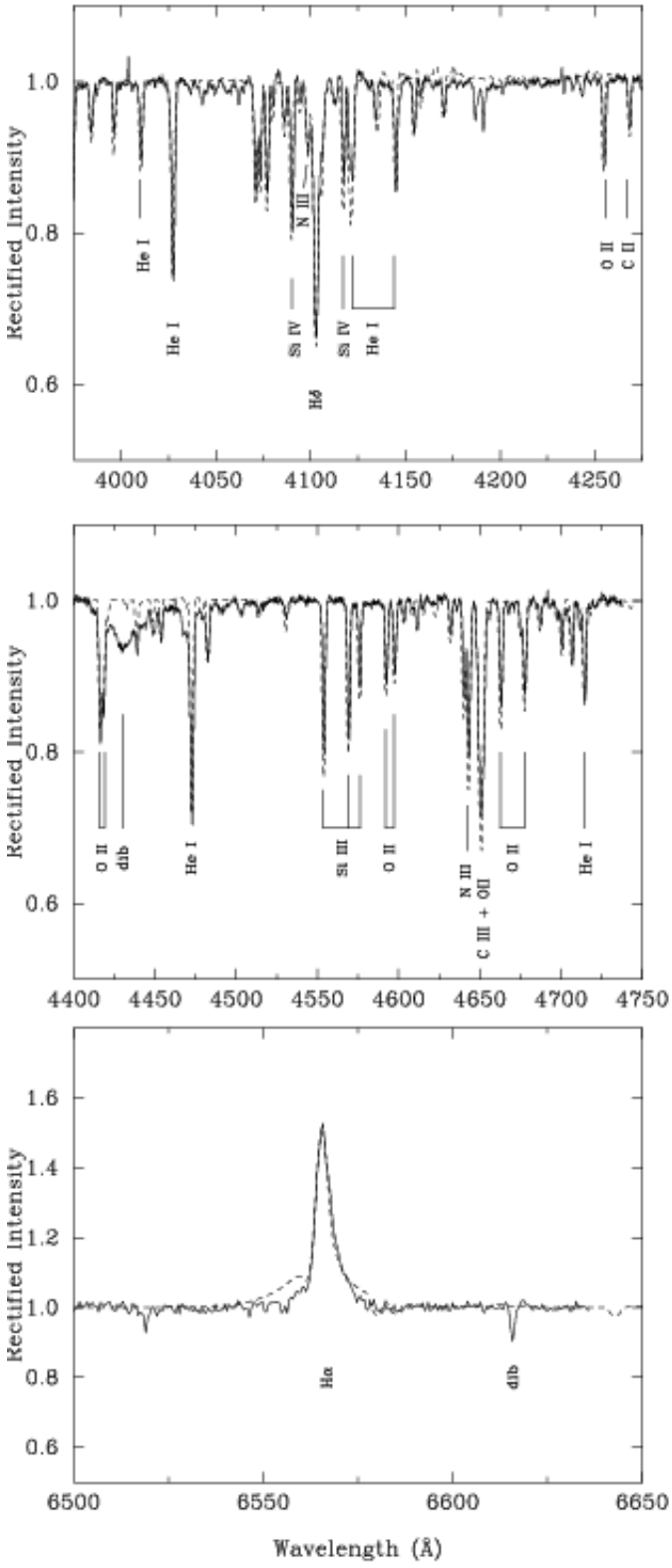

Fig. 12.— Comparison of the HD 2905 optical data with the model fit (dashed line) in the two primary diagnostic blue regions and in the vicinity of Hα. From blue to red wavelengths, by species, the labelled lines are: He I $\lambda\lambda$4009, 4026, 4116, 4121, 4144, 4471, 4713; C II λ4267; N III $\lambda\lambda$4097, 4640; O II $\lambda\lambda$4255, 4415-17, 4591-96, 4661-73-76; Si III λ4553-68-75; Si IV

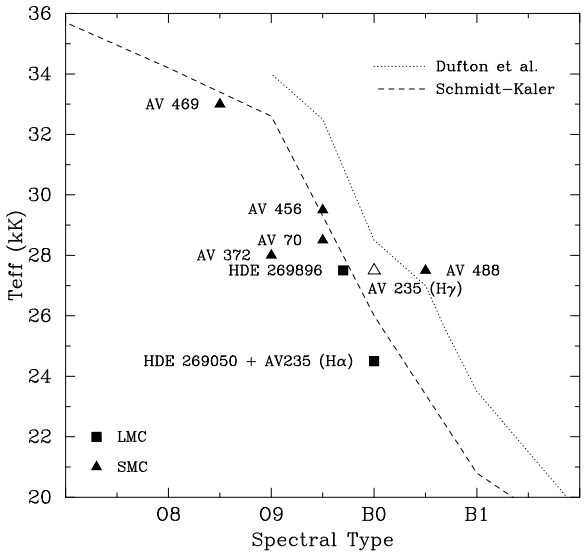

Fig. 13.— Comparison of derived temperatures with selected calibrations for our current targets in the LMC (squares) and SMC (triangles). Also shown are published temperature scales from Schmidt-Kaler (1982; dashed line) and Dufton et al. (2000; dotted line).

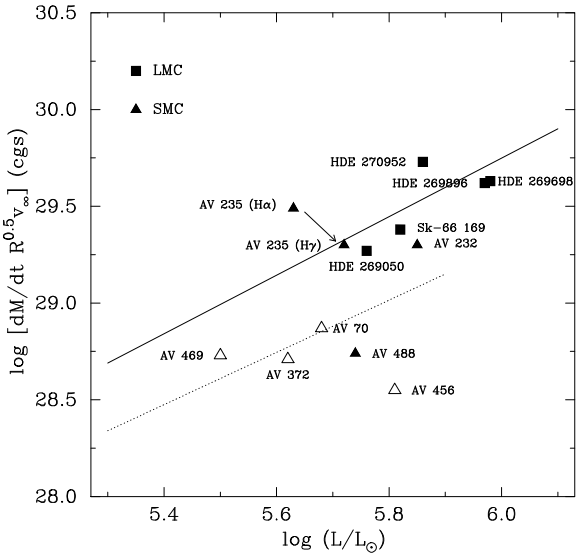

Fig. 14.— Reduced wind momentum as a function of luminosity for both the current sample and the four stars from Paper I. The type Ia stars are shown as solid symbols, the less luminous stars as open symbols. The form of the wind-momentum-luminosity relationship for Galactic O and early B-type supergiants (solid and dotted lines respectively) from Kudritzki & Puls (2000) are shown. Two values are shown for AV 235, based on (homogeneous) mass-loss rates obtained from Hα and the Hγ (see §5).

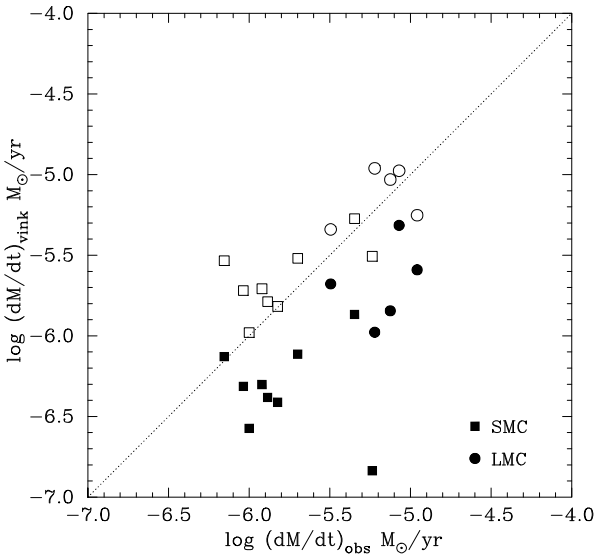

Fig. 15.— Comparison between theoretical (Vink et al., 2001) and observed (unclumped) mass-loss rates for our sample. Open symbols are theoretical values calculated for $Z/Z_{\odot} = 1$, while solid symbols indicate computed values for LMC ($Z/Z_{\odot} = 0.4$; circles) and SMC ($Z/Z_{\odot} = 0.2$; squares) metallicities. The dotted line highlights the 1:1 relationship.